This is to certify that the

thesis entitled

SPECTROSCOPIC STUDIES OF SOME
MODEL KETOPORPHYRINS

presented by

Gabriel Boktos

has been accepted towards fulfillment
of the requirements for

M.S. degree in Chemistry

Major professor

Date February 20, 1981

SPECTROSCOPIC STUDIES OF SOME MODEL KETOPORPHYRINS

By

Gabriel Boktos

A THESIS

Submitted to
Michigan State University
in partial fulfillment of the requirements
for the degree of

MASTER OF SCIENCE

Department of Chemistry

1981

ABSTRACT

SPECTROSCOPIC STUDIES OF SOME
MODEL KETOPORPHYRINS

By

Gabriel Boktos

Absorption, resonance Raman and infrared spectroscopies were employed to study the carbonylated derivatives of chlorins and isobacteriochlorins, viz. Cu-gemini monoketoporphyrin, Cu-gemini diketoporphyrins, and Cu-α, γ-dioxoporphodimethene. This investigation focused on the observation of the stretching frequency and on the effect of the position of the carbonyl(s) on the macrocyclic ring on the electronic and vibrational spectra.

Resonance Raman spectroscopy also provided information concerning the stretching frequencies of the $C_\alpha C_m C_\alpha$ and C_β-C_β bonds, the location of the carbonyl and how the perturbation by the carbonyl substituents relates to the overall structure of the molecule. These studies indicate that the positioning of the carbonyls around the pyrrole rings has only negligible effect on the $C_\alpha C_m C_\alpha$ stretching frequency. However, the C_β-C_β bond is perturbed by the carbonyl substituent(s) as exemplified by the great fluctuation of the C_β-C_β stretching frequency between 1567-1583 cm^{-1}.

The infrared spectra also provided information about carbonyl stretching. The non-splitting or splitting of the infrared peak was attributed to the existence or lack of a mirror plane through the molecule, which makes the carbonyls equivalent or non-equivalent respectively. The infrared studies thus supported and supplemented the resonance Raman results.

Finally, two additional compounds: Cu-transoctaethyl-chlorin [Cu(OEC)] and Cu-3,13-diformyl,8,18-di-n-pentyl-2, 7,12,17,-tetramethylporphine [Cu(2F-6F) for short] were introduced for purposes of comparison. Raman spectra of both were obtained under Soret excitation. In Cu(OEC) vibrations above 1300 cm^{-1} are intensified under these conditions, in contrast to intensification of lower frequency modes under Q-band excitation. The characteristic C=O vibrations in Cu(2F-6F) and Cu(2-6) diketo differ by more than 35 cm^{-1}; thus the formyl and ketone groups are easily distinguished in the substituted porphyrins.

equivalent or non-equivalent respectively. The infrared

Dedicated to my mother.

ACKNOWLEDGMENTS

I would like to acknowledge the contributions of Professors George E. Leroi and Gerald T. Babcock, under whose guidance and support I completed this undertaking.

In addition, the help of Professor Chris Chang, coupled with the preparative work by Richard Young, is gratefully appreciated and acknowledged.

I would also like to express my gratitude to fellow students who took the time to converse with me and exchange ideas. So to B. Ward, J. McMahon, R. Blevins and to all my compatriots I express my deep appreciation and a big thanks.

Finally, a special thanks to Margy Lynch and Beverly Adams, who ably and cheerfully helped in the preparation of this manuscript.

I would like to acknowledge the contributions of

TABLE OF CONTENTS

LIST OF TABLES

LIST OF FIGURES

ABBREVIATIONS

RRS:	Resonance Raman Spectroscopy (Spectra)
IRS:	Infrared Spectroscopy
Cumonoketo:	Cu-gemini monoketoporphyrin or Cu-gemini porphoketone
Cu(2-3):	Cu-2, 3-gemini diketoporphyrin or Cu-2, 3-gemini porphodiketone
Cu(2-4):	Cu-2, 4-gemini diketoporphyrin
Cu(2-5):	Cu-2, 5-gemini diketoporphyrin
Cu(2-6):	Cu-2, 6-gemini diketoporphyrin
Cu(OEC):	Cu-transoctaethyl chlorin
Cu(OEP):	Cu-octaethylporphyrin
Cu(2F-6F):	Cu-3, 13-diformyl,8,18-di-n-pentyl-2,7,12, 17,-tetramethylporphine
Fe(2F-4F):	2,4-diformyl-iron protoporphyrin IX
Cu(α-γ):	Cu-α,γ-dioxo-porphodimethene

RRS: Новогодняя Ярмарка Электроскоу (Spectra)

CHAPTER 1

Introduction

One of the major challenges of modern biochemistry has been the elucidation of biological function in terms of molecular structure. Numerous spectroscopic methods have been introduced to monitor structural features and detect changes which accompany biological function. Among them, vibrational spectroscopy offers high expectations, since vibrational frequencies available from infrared or Raman spectra are sensitive to bonding and geometric arrangements of localized groups of atoms in a molecule.

Among molecules of biological importance, metalloporphyrins and metallochlorins are two of the best candidates. Metalloporphyrins are essential to the life of plants, animals, fungi and bacteria. Metallochlorins appear in many forms such as chlorophylls, or as gemini ketoporphyrins, which have been recently synthesized in our bioorganic lab by Professor Chris Chang. These molecules are of biological importance because they are related to synthetic analogues of sirohydrochlorin which is the demetallated siroheme prosthetic group of nitrite and sulfite reductase. The synthesis of the gemini diketoporphyrins involves the oxidation of octaethylporphin using hydrogen peroxide. Each diketoporphyrin was then separated and purified by

chromatography.

Experimental

In this particular project the techniques employed were absorption, infrared, and resonance Raman spectroscopies. The optical spectra were taken by using a Cary 17 spectrophotometer in the visible and ultraviolet regions in order to obtain both the Q and Soret bands. The infrared spectra were recorded using a Perkin Elmer 283 B Infrared spectrophotometer, with 0.1 mm (cavity) cells. Resonance Raman spectra of Cu-gemini-ketoporphyrins in CH_2Cl_2 were recorded by using two Soret lines (406.7 and 413.1 nm) from a Spectra Physics 164-11 Kr ion laser in conjunction with a Spex 1401 double monochromator and associated Ramalog electronics. A prism, external to the laser cavity, was utilized in order to separate the two frequencies. The rotating cell technique was also used to avoid the local heating of the samples. (See Figure 1a for schematic representation.)

The compounds were obtained from our biorganic lab and they were 80-95% purity. The solutions used were 5-30 μmolar in CH_2Cl_2. Visible excitation (488.0 nm, 514.5 nm) was also employed but fluorescence obscured the weakly-enhanced Raman scattering; therefore Q-band excitation was abandoned.

absorption, infrared, and reemission using spectroscopies.

The optical spectra were taken by using a Cary 17 spectro-

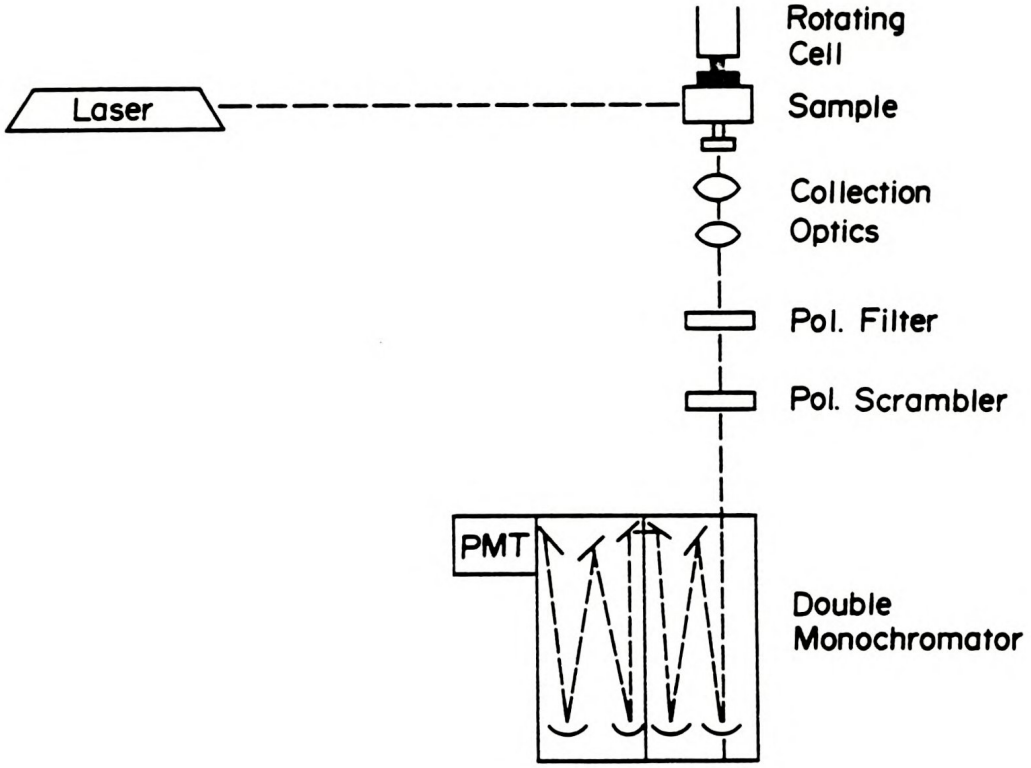

Figure 1a. Schematic representation of laser Raman experimental arrangement.

CHAPTER 2

A. ABSORPTION SPECTRA OF CHLORINS AND RELATED COMPOUNDS

1. Some theoretical aspects of heme absorption

In general, the electronic absorption spectra of porphyrins and related compounds are dominated by two strong transitions as in Figure 1b [1]. The transition in the 500-700 nm visible region is referred to as the Q-band, whereas the more intense transition in the near uv region at approximately 400 nm is the Soret, or B-band. Between the B and Q transitions there is a satellite band (on the Q-band) which arises from the vibronic mixing of bands B and Q [2,3]. Many times there is a plethora of bands between these two main bands, arising from the perturbation of the centrosymmetric cyclic model due to lowering of symmetry or the existence of peripheral substituents on the ring as in Figure 1c [4]. The 16-member cyclic polyene mentioned above is a convenient model for the treatment of porphyrin absorption spectra [4].

Simpson [5] was the first to discuss the porphyrin spectra. His approach was based on a successful free-electron-model, characterized by the assumption that the π-electrons of porphin are free particles on a 16-lattice atom ring, providing a conjugated electron current. In this model, the 18 π-electrons are paired in orbitals of

A. ABSORPTION SPECTRA OF CHLORINE AND RELATED COMPOUNDS

1. The Theoretical Equation

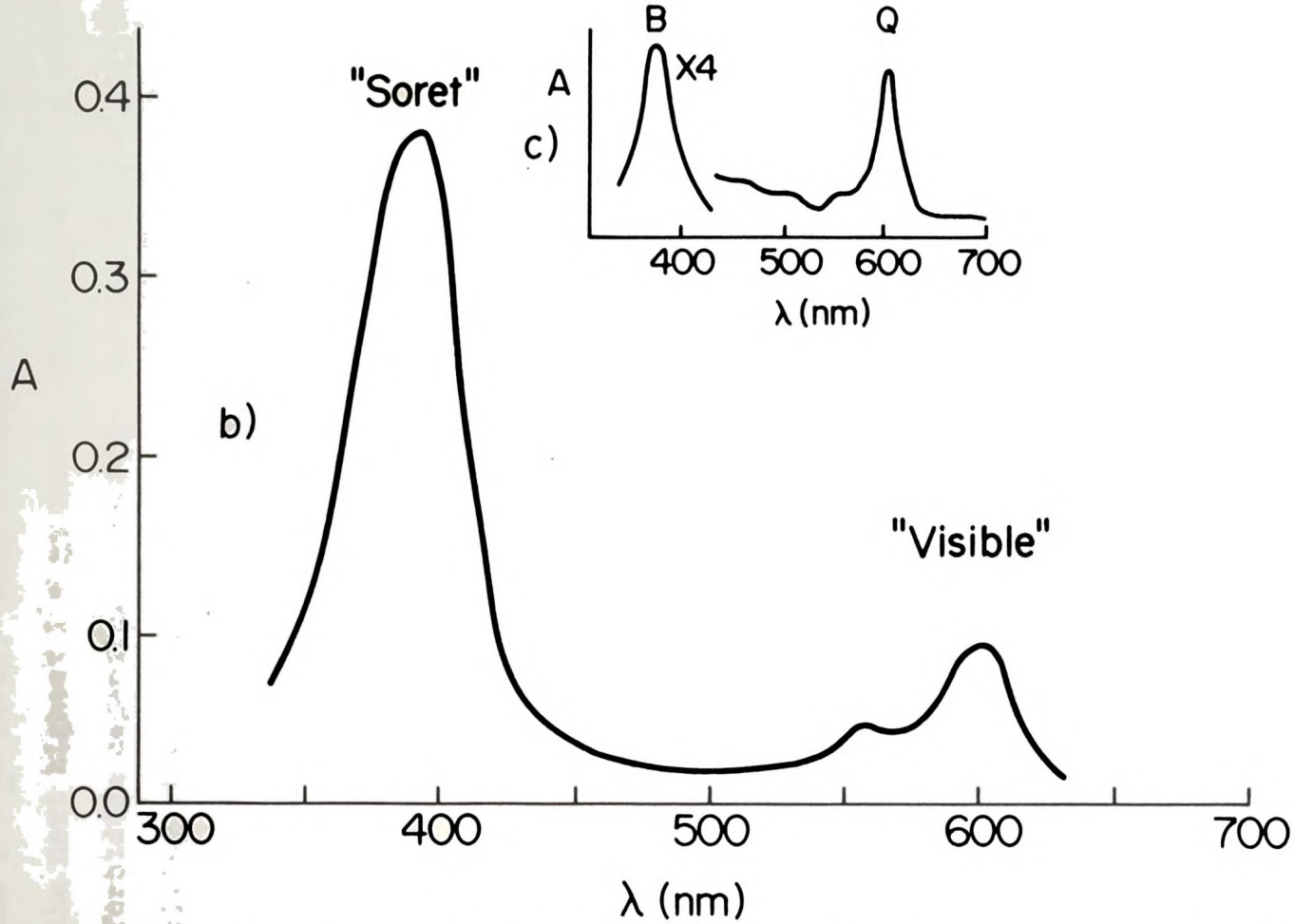

Figure 1. b.) Optical spectra of Ferrocytochrome C in CH_2Cl_2 (conc. 0.5 mM)
c.) Optical spectra of Fe(OEC)Cl. C in CH_2Cl_2 (conc. 0.3 mM)

increasing angular momentum with the system filled up to the $l = \pm 4$ level. When a transition occurs from $l = \pm 4$ to the next highest $l = \pm 5$ level, then it can be allowed or forbidden depending on whether $\Delta l = \pm 1$ or $\Delta l = \pm 9$, thus giving rise to the B and Q bands respectively.

A more detailed and explanatory model, first introduced by Moffitt [4], Platt [6] and later presented by Gouterman [7], considered only the two highest filled cyclic polyene orbitals as shown in Figure 2. This model which was also reaffirmed by a number of Russian spectroscopists [3,8] is the famous "four orbital model". The two lowest unfilled orbitals are the degenerate e_g states, whereas the two highest filled orbitals also can be accidentally degenerate, which is a rather general argument pertaining in many cases. The spatial shape and nodal characteristics of these four orbitals are shown in Figure 3 for purposes of comparison.

There are basically two doubly-degenerate MO configurations [9], $(a_{1u})^2 (a_{2u})^1 (e_g)^1$ and $(a_{1u})^1 (a_{2u})^2 (e_g)^1$ for the two lowest excited states of the π -electrons emanating from the porphyrin ground state configuration $(a_{1u})^2 (a_{2u})^2$. It has been shown [10] that these two singly-excited configurations give equally mixed linear combinations, as a result of configuration interaction. Therefore, the x and y components of the Q and B states can be extracted from the relationships involving the CI parameter α and the appropriate 50/50 mixtures of the excited configurations Q_x^0, Q_y^0, and B_x^0 and B_y^0 as follows:

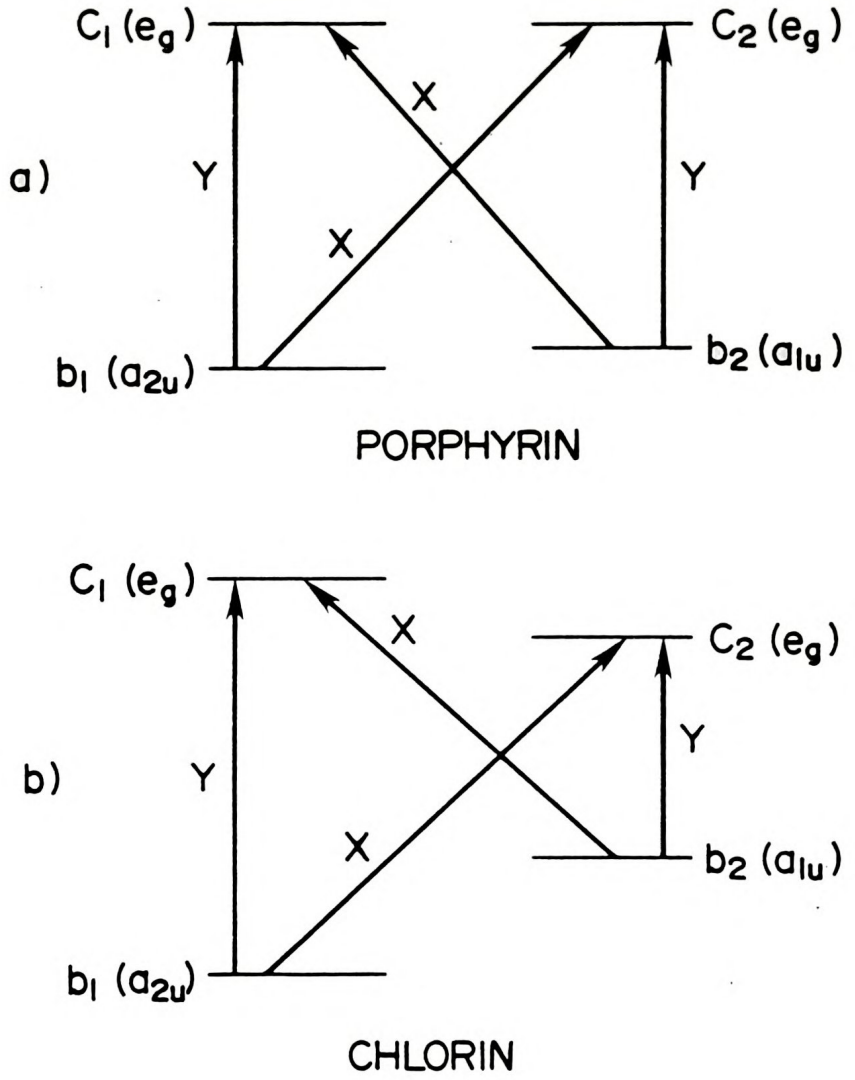

Figure 2. Four orbital model (from reference # 7)

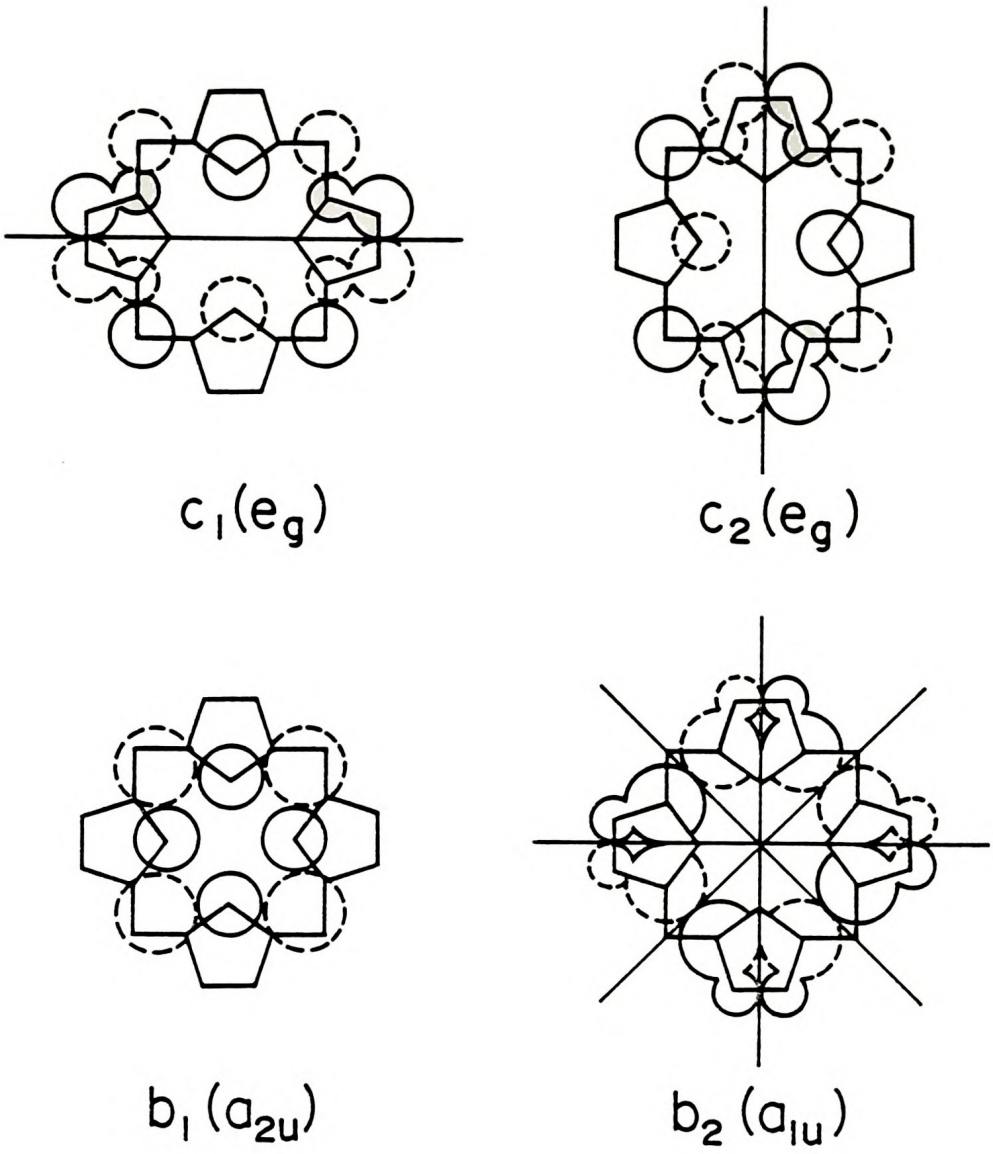

Figure 3. Shape and nodal characteristics of the four orbitals. (from ref. # 7)

$$|Q_x> = \cos\alpha\,|Q_x^0> - \sin\alpha\,|B_x^0>$$

$$|Q_y> = \cos\alpha\,|Q_y^0> - \sin\alpha\,|B_y^0>$$

$$|B_x> = \cos\alpha\,|B_x^0> + \sin\alpha\,|Q_x^0>$$

$$|B_y> = \cos\alpha\,|B_y^0> + \sin\alpha\,|Q_y^0>. \qquad (2.1)$$

Parameter α was demonstrated to unmix the configurations, and it differs for each central metal and porphyrin complex. Gouterman [8] pointed out that consideration of the various factors which influence α can give very fruitful results with regards to the properties of porphyrin absorption or emission spectra.

The Q^0 and B^0 components are:

$$Q_x^0 = \frac{\sqrt{2}}{2}\,[a_{2u}e_{g_x} + a_{1u}e_{g_y}]$$

$$Q_y^0 = \frac{\sqrt{2}}{2}\,[a_{2u}e_{g_y} - a_{1u}e_{g_x}]$$

$$B_x^0 = \frac{\sqrt{2}}{2}\,[a_{2u}e_{g_x} - a_{1u}e_{g_y}]$$

$$B_y^0 = \frac{\sqrt{2}}{2}\,[a_{2u}e_{g_y} + a_{1u}e_{g_x}] \qquad (2.2)$$

2. Results

Metallochlorins [11] differ from metalloporphyrins [12-15] merely by the reduction of one C_β - C_β bond of a pyrrole ring in the conjugated macrocycle; however, this gives rise to distinctly different absorption spectra.

Isochlorins and bacteriochlorins, which have two saturated C_β - C_β bonds, also exhibit electronic spectra with great differences in comparison with metallochlorins and metalloporphyrins.

Two consequences in the absorption spectra follow when changing from a porphin to a chlorin, with the consequent lifting of the degeneracy of the lowest excited configurations (Figures 2 and 4): (1) the spectrum and mainly the Q band shifts to the red, and (2) the Q_y band intensifies as in Figures 5, 7, 8, 10, and 11. However, the Q_x band of chlorins is not strengthened sufficiently to stand out from the vibrational overtones of Q_y [16]. Both consequences mentioned above have been quantitatively shown by Platt [17,18] and later by Gouterman [8], who predicted that the "true" measure of intensity is the dipole strength q^2 (in square Angstroms) given by:

$$q^2 = \frac{1}{2500} \varepsilon \frac{\Delta\lambda}{\lambda}$$

where λ is wavelength of band-peak, $\Delta\lambda$ is the halfwidth and ε is molar extinction coefficient of the sample in that particular region.

The chlorin Soret band is found at almost the identical energy as that of porphin and its B_x and B_y components are almost degenerate in unsubstituted metal chlorins. Hence, the CI pattern of chlorin as well as its spectrum likely resemble those of tetrabenzaporphin [19-22].

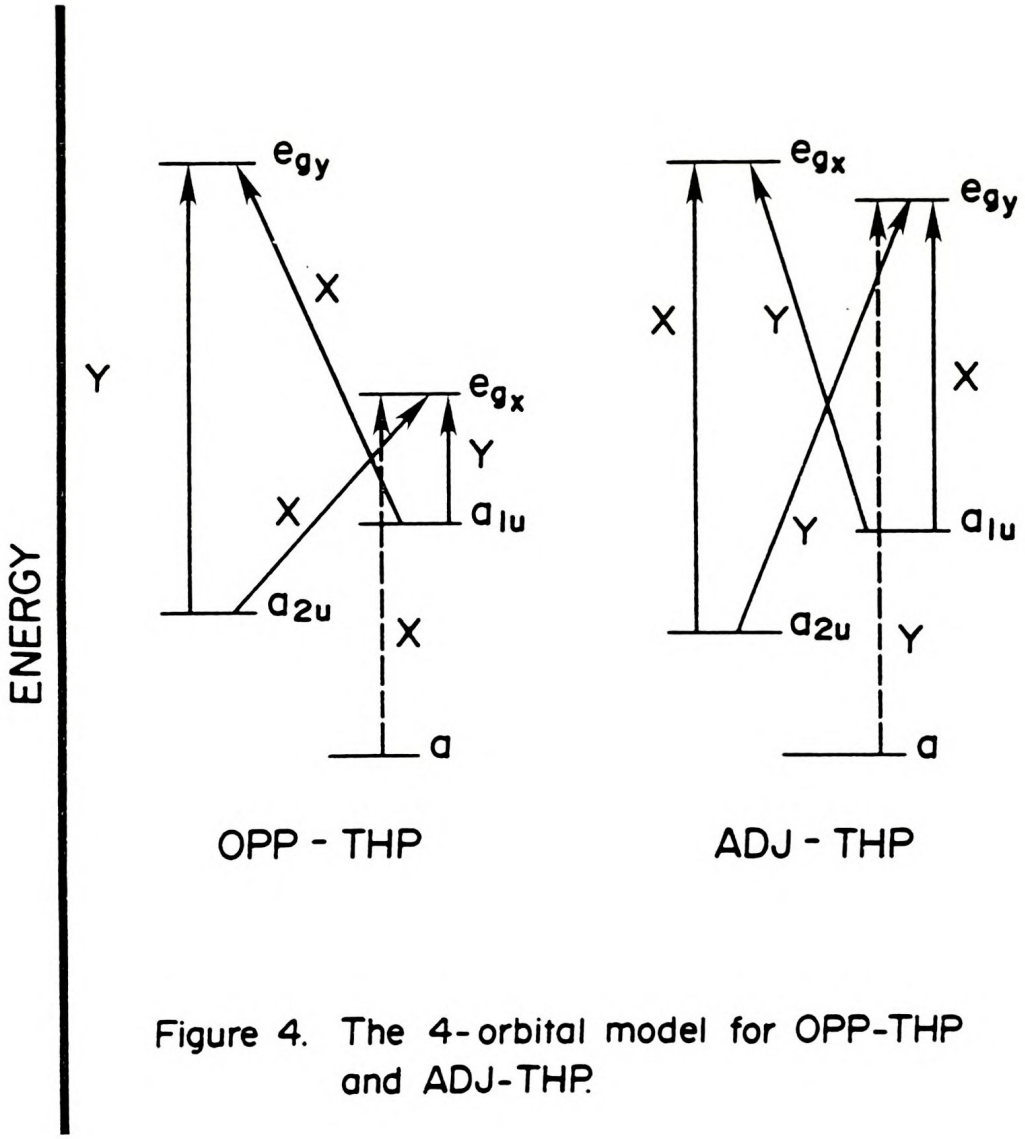

Figure 4. The 4-orbital model for OPP-THP and ADJ-THP.

The x-allowed states, which are not constrained by symmetry, appear to be lowered by CI more than y-allowed states. Some calculations performed by McHugh et al. [23] indicate that the Soret band of free base chlorins includes three major allowed electronic transitions as in free-base porphin.

Another very prominent feature of the chlorin substituted spectra is the "split" Soret. This phenomenon is due to the presence of an electron-withdrawing group such as a carbonyl directly attached to the pyrrole ring - which makes forbidden transitions allowed. These bands arise from transitions between B and N states. The N band itself, as seen in Figure 4, arises from transitions between the "a" orbital and the e_g orbital. The "a" orbital which lies below the a_{1u} and a_{2u} orbitals is a descendant of a cluster of closely spaced orbitals such as $2a_{2u}$ and $2b_{2u}$ of porphin. The bands that arise from the coupling of B and N are indicative of the new $\pi - \pi^*$ state which involves the electron-withdrawing group. They were also observed and identified by Caughey et al. [24] in the spectra of metal 2,4-diacetyldeutero-porphyrins.

A brief assignment of the visible and uv spectra follows:

a) The Cu(OEC) optical spectra, as shown in Figure 5, exhibit an intense band at approximately 615 nm, assignable according to Gouterman [7], to the $Q_y(0\text{-}0)$ transition, whereas the remaining weak bands around 500-600 nm are

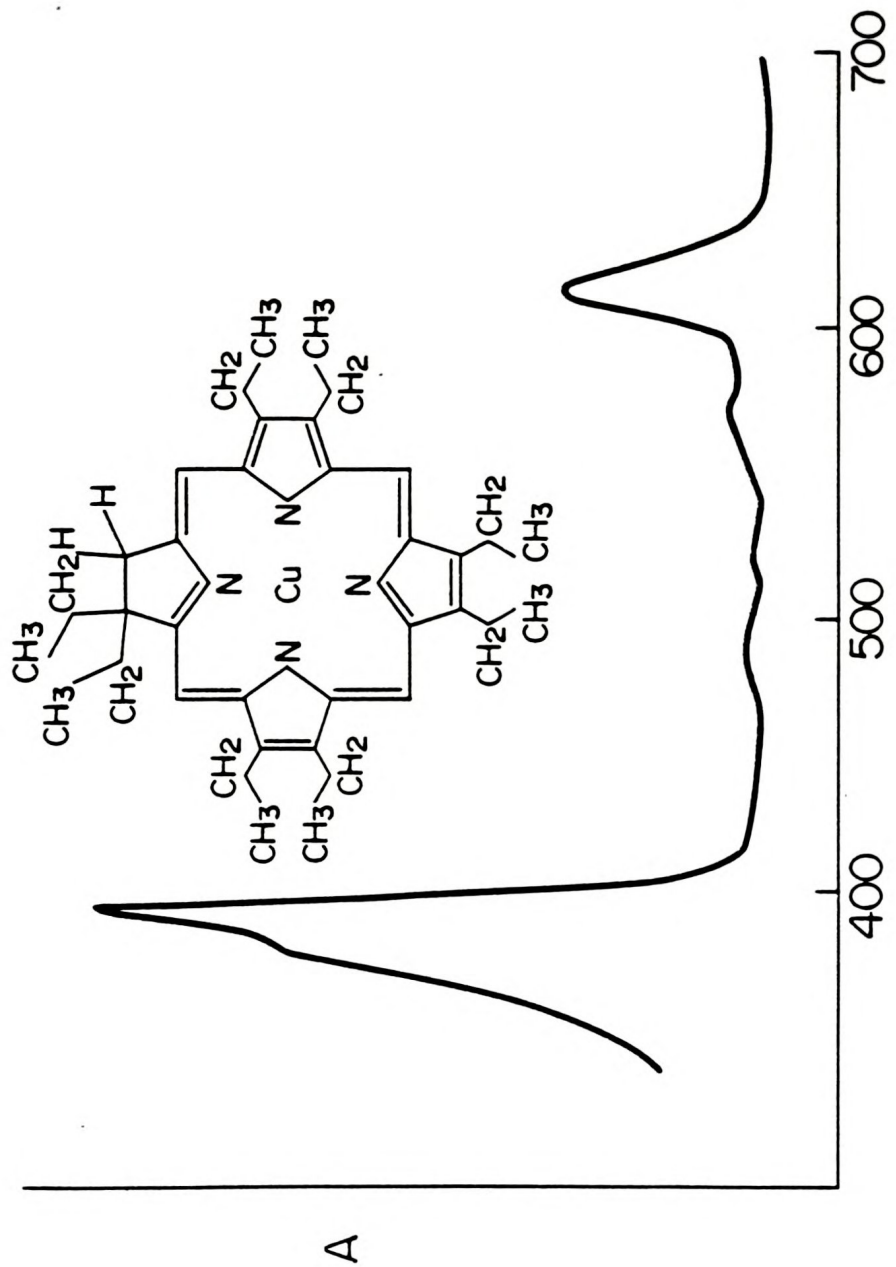

Figure 5. Optical spectra of Cu(OEC).

assignable to the $Q_x(0\text{-}0)$ and the $Q_y(0\text{-}1)$ and $Q_x(0\text{-}1)$ transitions. The Soret band appears at 400 nm with a weak shoulder to the blue, possibly arising from the lowering of symmetry by the saturation of one C_β - C_β bond in Cu(OEC). The Cu(OEC) absorption spectra recorded here are in agreement with the spectra of Fe(OEC)Cl and [Fe(OEC)Im_2]Cl and in general of M(OEC), recorded by Kitagawa previously [25].

b) The absorption spectra of 2F - 6F are shown in Figure 6. Due to the presence of the electron-withdrawing formyl groups on positions 2 and 6, both Soret and Q bands are shifted to the red as in cytochrome oxidase [26] and in 2-4 diformyl iron protoporphyrin IX [27].

The visible bands appear at 615, 580, 560 and 510 nm. The lowest energy band at 615 nm probably corresponds to the $Q_y(0\text{-}0)$ transition. The other three bands appear to be extremely weak - especially the 580 and 560 nm bands - which indicates cancellation of the dipole moments for the corresponding transitions.

The Soret is very sharp but slightly split at 420 nm and 415 nm, which possibly signifies the presence of the two formyl groups.

c) The Cu-monoketo spectrum illustrated in Figure 7 clearly exhibits the "chlorin type" absorption. The two most important features are the very intense $Q_y(0\text{-}0)$ band at 618 nm and the strong "split type" Soret band at 415 nm. The $Q_y(0\text{-}0)$ band is also accompanied by two - and not four - not very well resolved humps at higher energies; 570 and 512 nm.

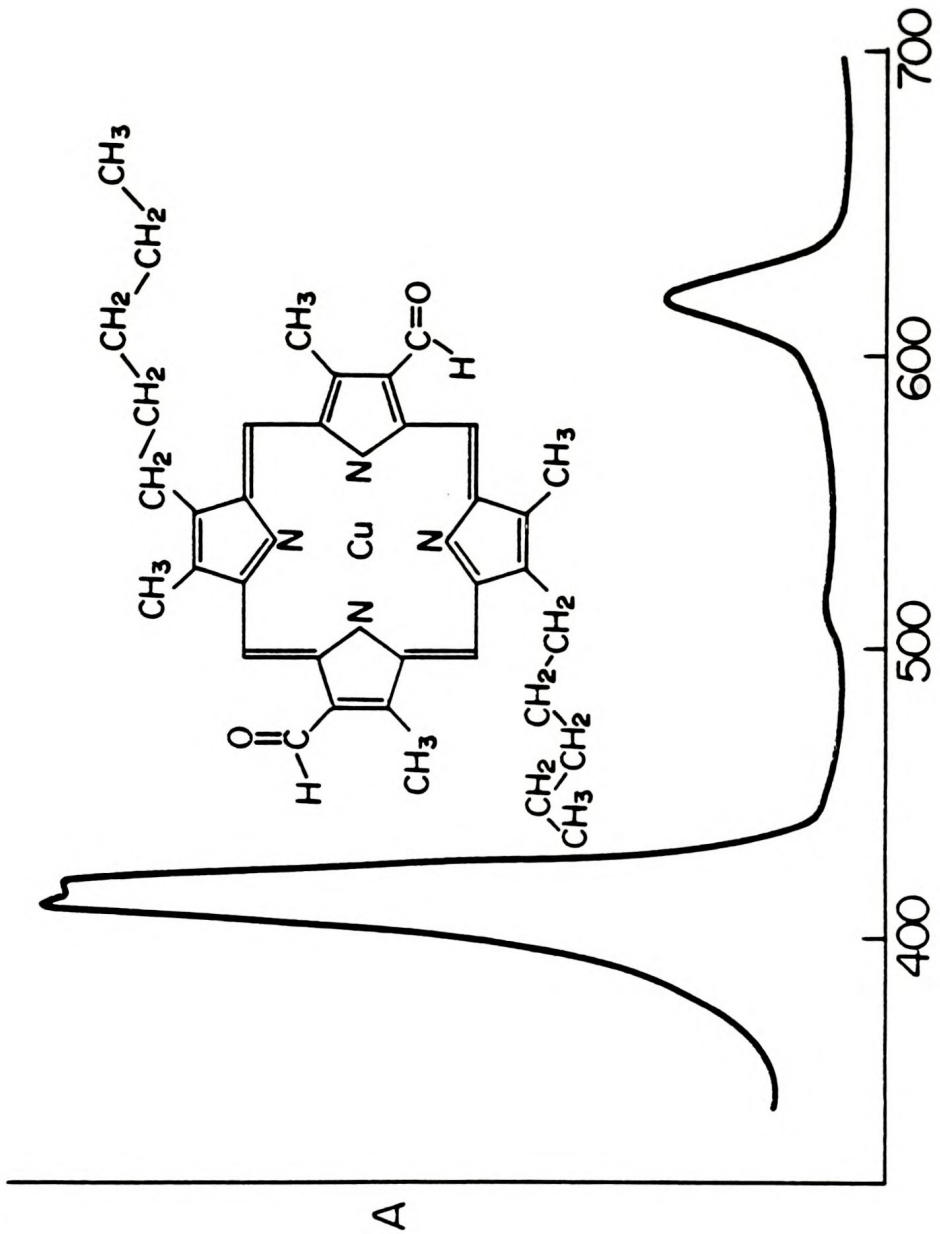

Figure 6. Optical spectra of Cu(2F-6F).

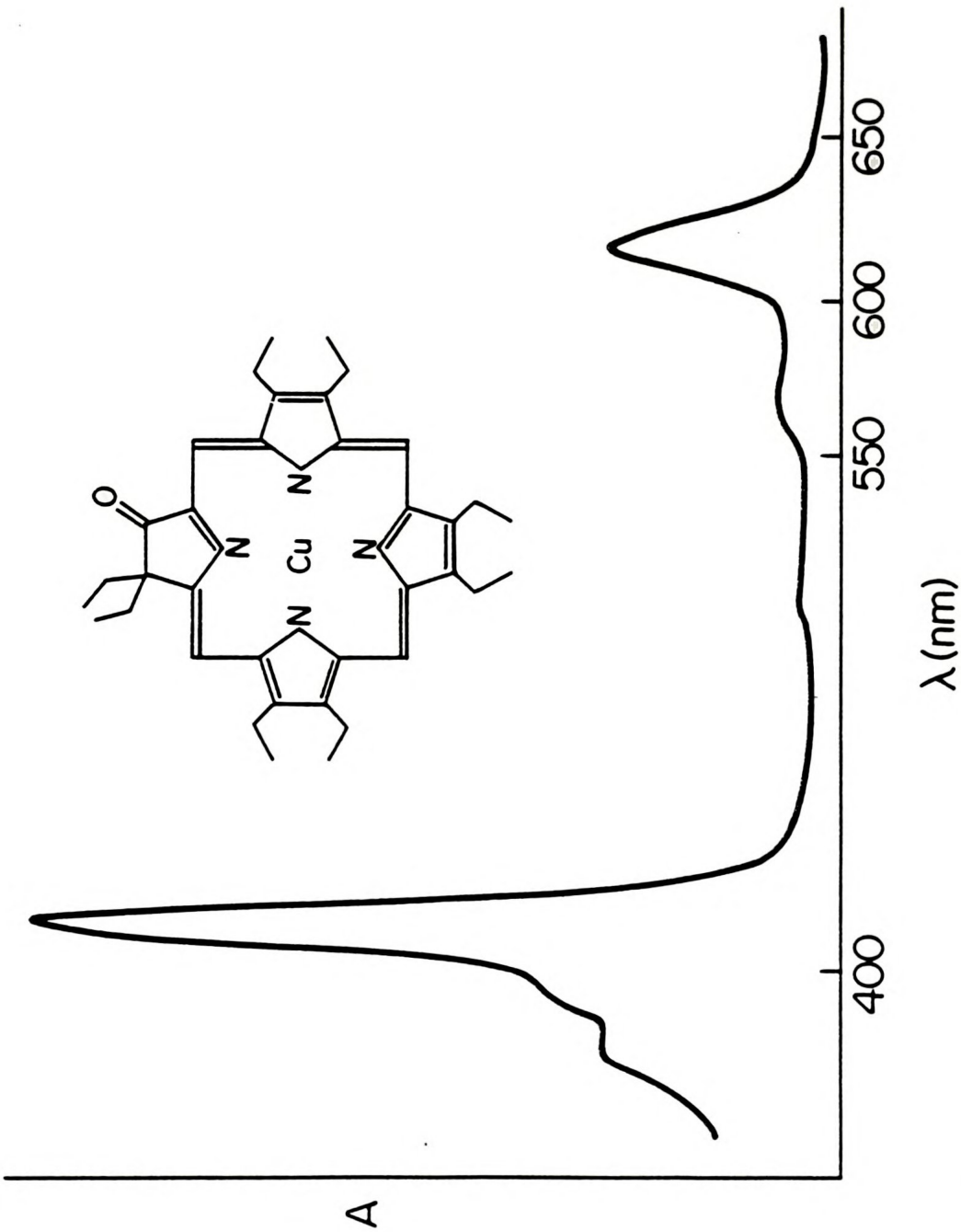

Figure 7. Optical spectra of Cu monoketo.

The most striking feature, however, if the multiple splitting of the Soret. This effect has been observed previously by Weiss [16], who concluded that the multiple splitting of the Soret band is attributable to the existence of a substituent on the porphyrin ring which lowers the symmetry and makes "forbidden" bands allowed. These bands, which appear in the spectrum at energies above that of the Soret band (see Figure 6), are forbidden in square (D_{4h}) symmetry.

d) As illustrated in Figure 8, the Cu(2-3) diketo spectrum is characterized by a very intense Q_y(0-0) transition at 688 nm and a dramatically "split Soret". Again the Q_y(0-0) transition is accompanied by three higher energy peaks at 630 nm, 580 nm and 540 nm. The 580 nm band appears to be somewhat more intense than either of the other two.

The experimental Soret band is rather complex. It shows three obvious components, at 442 nm, 430 nm and 395 nm, with the middle component being most intense. This pattern of splitting is again attributable to the existence of two carbonyls on two adjacent pyrroles.

Another striking effect to be observed in the Cu(2-3) diketo spectrum is the dramatic shift of the Q_y(0-0) band to 688 nm, and also its increase in intensity relative to the Soret intensity.

e) The Cu(2-4) diketo optical spectrum is shown in Figure 9. The most obvious characteristic of the spectrum is the band which lies farthest to the red. This band,

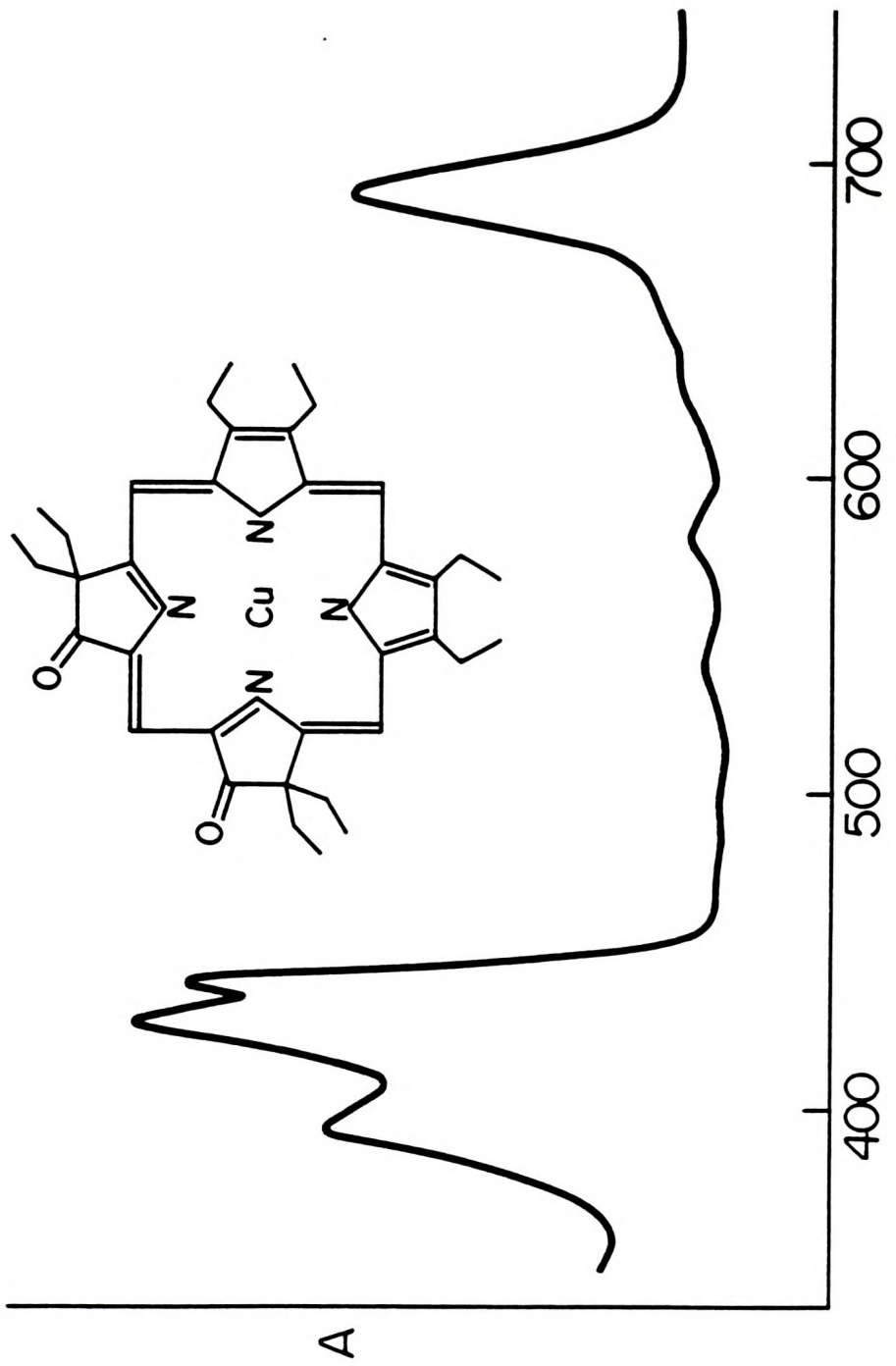

Figure 8. Optical spectra of Cu(2-3) diketo.

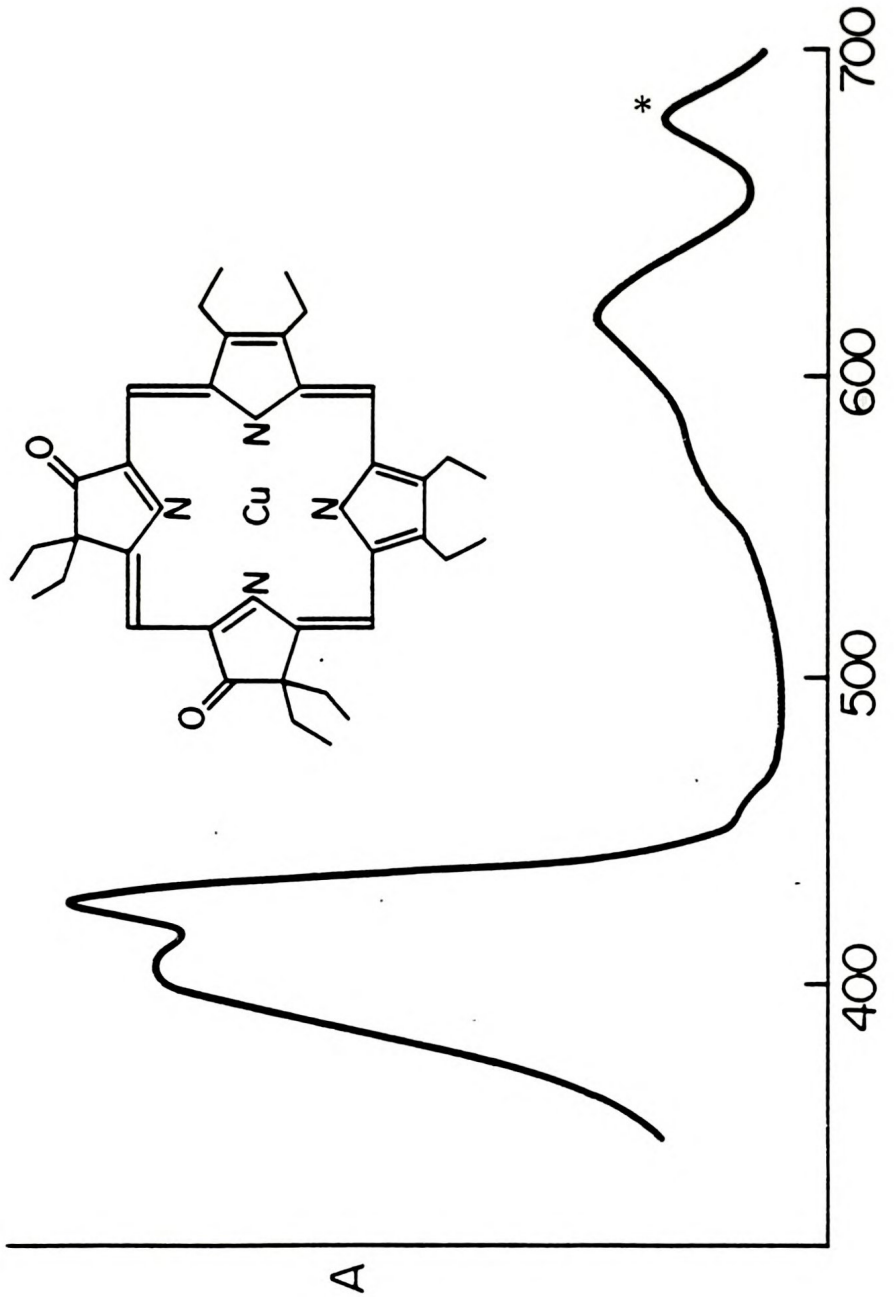

Figure 9. Optical spectra of Cu (2-4) diketo. (* notice anomaly)

which has been assigned [9] to the $Q_y(0\text{-}0)$ transition, is of lower intensity than the band to its blue. Due to this anomaly we will refrain from any discussion of this particular optical spectrum.

f) Figure 10 illustrates the spectrum of Cu(2-5) diketo, where the two carbonyls are on opposite pyrroles. Again, the two most prominent features of the spectrum are the very intense $Q_y(0\text{-}0)$ band and the quadruply split Soret. The Q transitions occur at 670 nm, 615 nm, 585 nm and 540 nm, whereas the Soret bands occur at 442 nm, and 420 nm, with two satellite bands at 398 nm and 380 nm.

In the visible region the band at 585 nm appears to be more intense than either the 615 nm or 540 nm bands. The same effect was previously seen by Seely [28] in the hexahydrotetraphenyl porphin spectra, and by Coyne et al., [29] in bacteriochlorphyll a. Magnetic circular dichroism studies that followed [30] assigned this band to the $Q_y(0\text{-}1)$ overtone.

The Soret band is the most dramatically split of all the observed spectra, which indicates tremendous lifting of the degeneracy where "forbidden" bands become "allowed".

g) Similarly, the Cu(2-6) diketo spectrum shown in Figure 11 reveals the same effect, particularly the increased intensity of $Q_y(0\text{-}0)$ in comparison to the Soret. The visible bands occur at 702 nm (the most highly intense and red shifted Q_y band of all the recorded spectra) and as small humps at 666 nm, 648 nm and 520 nm.

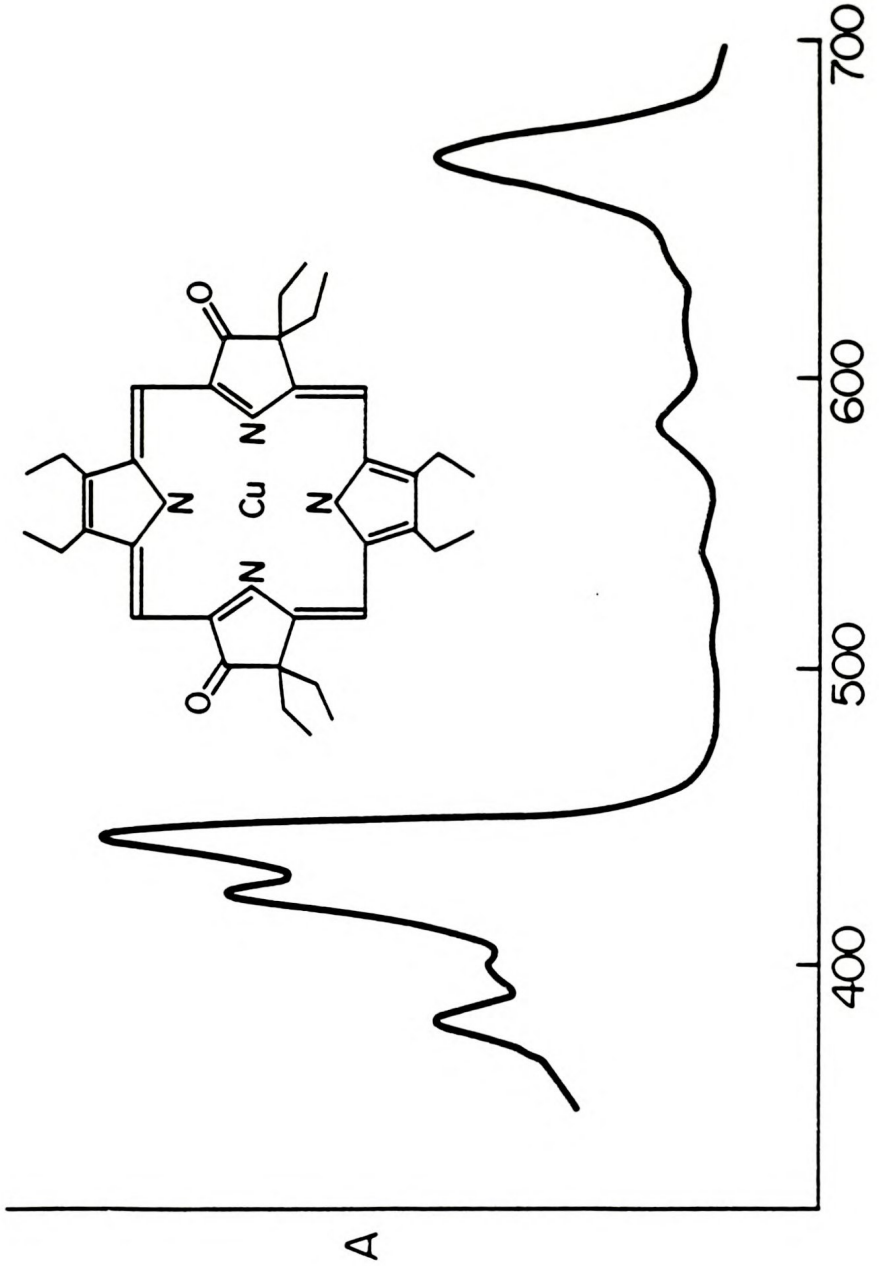

Figure 10. Optical spectra of Cu (2-5) diketo.

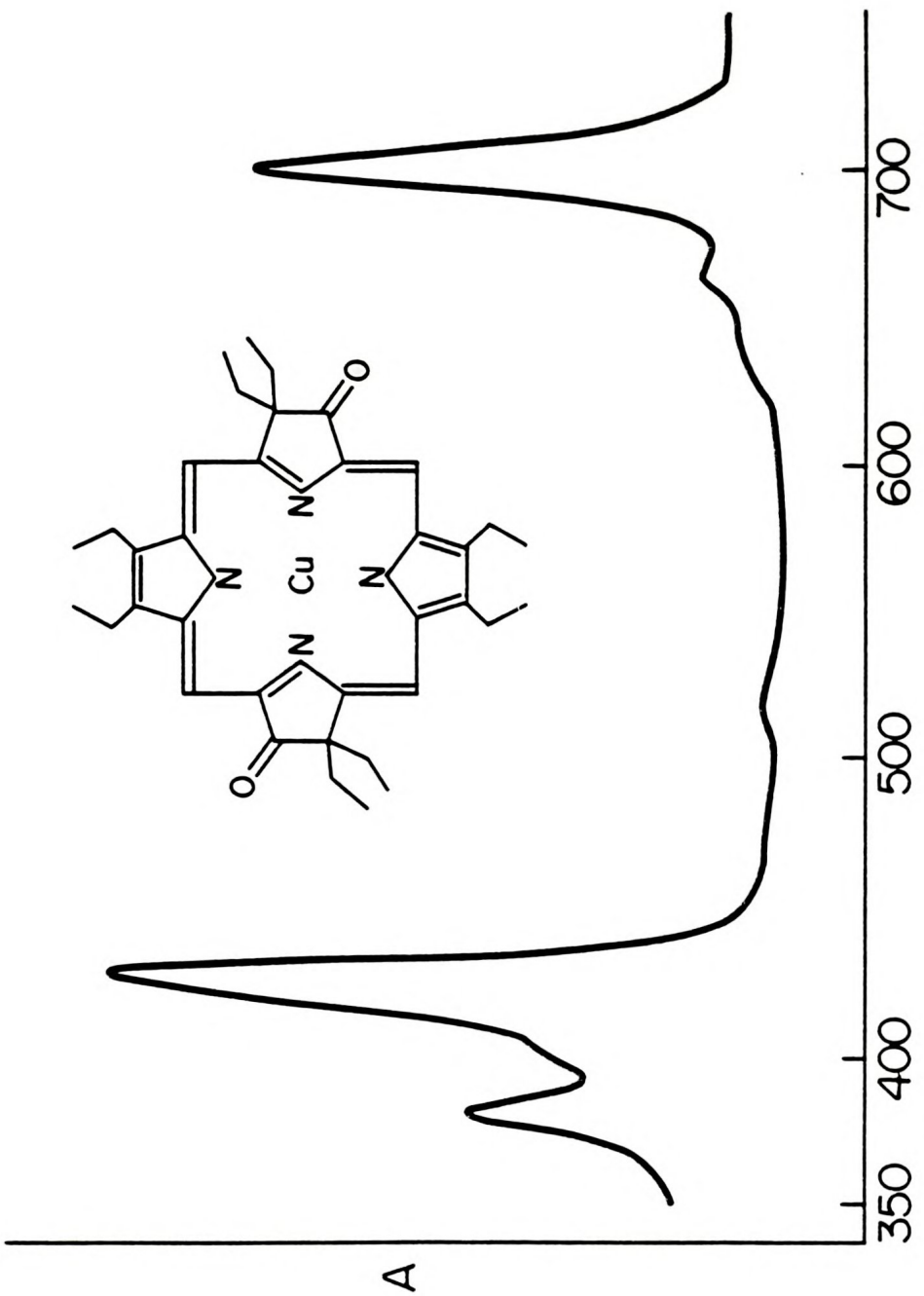

Figure 11. Optical spectra of Cu (2-6) diketo.

The Soret is doubly split into a very intense component at 427 nm - with a shoulder to its blue at 400 nm - and a weaker component at 380 nm. Again, this spectrum needs further investigation by fluorescence [31] and MCD [38] studies.

h) Finally, the Cu (α-γ) dimeso spectrum shown in Figure 12 is atypical of chlorin and typical of porphin spectra, with a rather broad Soret band at 440 nm and a visible transition at 600 nm, with a satellite band at 560 nm.

The Soret band is more intense than the low energy Q band and very broad, possibly due to the burial of one weak B component within the other. The most interesting feature, however, is the very slight hump at 400 nm. This hump could signify the existence of an electron-withdrawing group attached to the ring. (The wavelengths and energies of the various absorption bands are listed in Table 1 for purposes of comparison.)

Now that the various transitions have been assigned, one may consider the relative positions of the bands in relation to the conjugation pathway of each molecule.

Note, first, that when two adjacent rings are reduced, such as in Cu(2-3) and Cu(2-4) diketo, the two x-polarized transitions are nearly equal in energy. The very distinct feature about the optical spectra of both of these compounds is the dramatic shifting of the Q_y band towards the red. This effect is clearly illustrated by the increase of the "box" - or of the conjugation pathway - to 22 π instead of

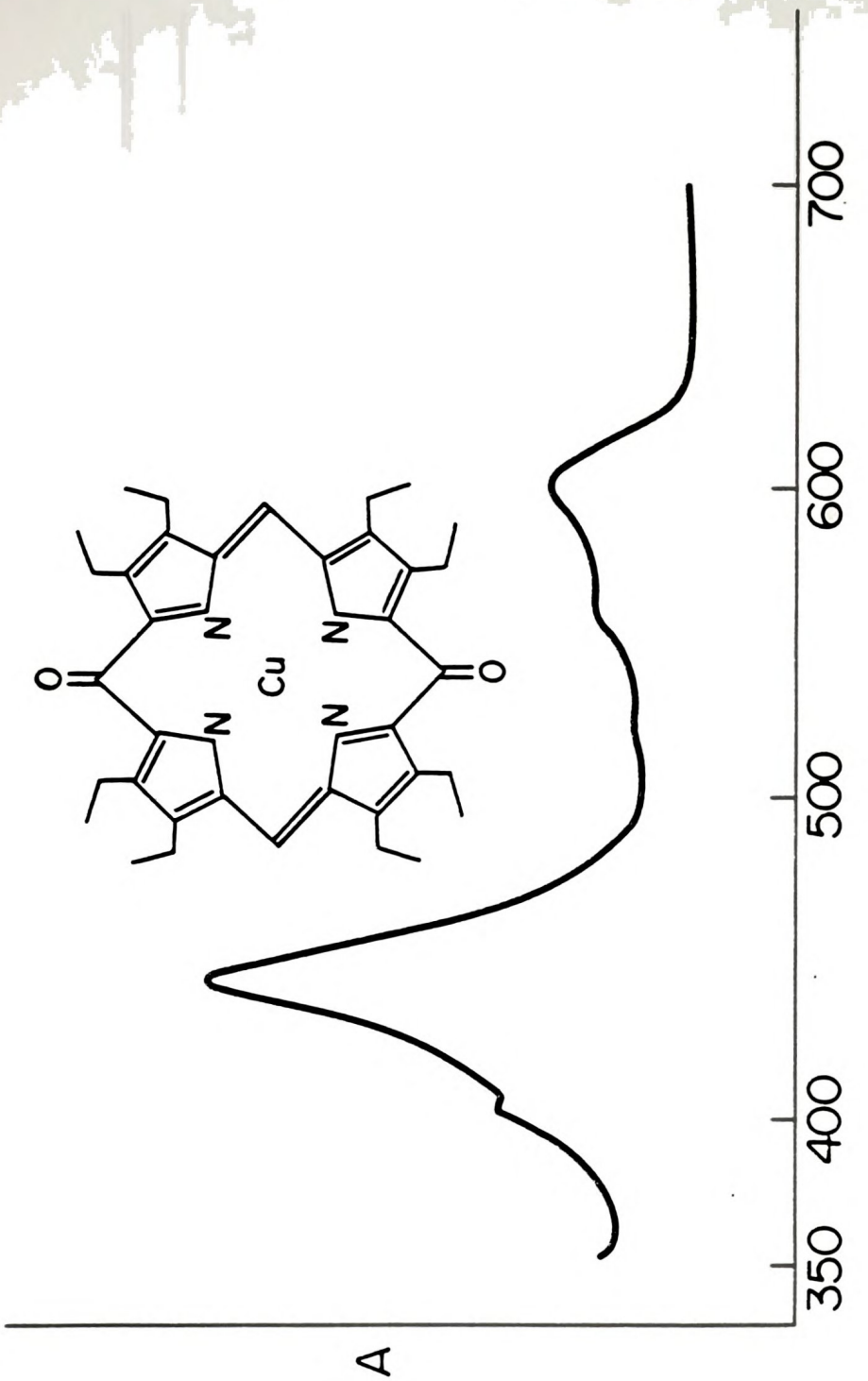

Figure 12. Optical spectra of Cu (α-γ) dimeso.

TABLE 1 - Energies and wavelengths of the chlorin electronic transitions.

Cu mono	Cu(2-3)	Cu(2-4)	Cu(2-5)	Cu(2-6)
600 nm 16666.667 cm^{-1}	688 nm 14534.884 cm^{-1}	688 nm 14534.884 cm^{-1}	670 nm 14925.373 cm^{-1}	702 nm 14245.014 cm^{-1}
560 nm 17857.143 cm^{-1}	630 nm 15873.016 cm^{-1}	600 nm 16666.667 cm^{-1}	615 nm 16260.163 cm^{-1}	666 nm 15015.015 cm^{-1}
415 nm 24096.386 cm^{-1}	580 nm 17241.379 cm^{-1}	545 nm 18348.624 cm^{-1}	585 nm 17094.017 cm^{-1}	648 nm 15432.099 cm^{-1}
	540 nm 18518.519 cm^{-1}	426 nm 23474.178 cm^{-1}	540 nm 18518.519 cm^{-1}	520 nm 19230.769 cm^{-1}
	442 nm 22624.434 cm^{-1}	405 nm 24691.358 cm^{-1}	505 nm 19801.980 cm^{-1}	426 nm 23474.178 cm^{-1}
	430 nm 23255.814 cm^{-1}		442 nm 22624.434 cm^{-1}	380 nm 26135.789 cm^{-1}
	395 nm 25316.456 cm^{-1}		420 nm 23809.524 cm^{-1}	
			398 nm 25125.628 cm^{-1}	
			380 nm 26315.789 cm^{-1}	

18 π, as illustrated in Figure 13.

On the other hand, the Cu(2-5) and Cu(2-6) spectra, where two opposite pyrrole rings I and III are reduced, exhibit an even more pronounced behavior (especially the Cu(2-6) diketo spectrum). In the latter, the Q_y(0-0) band is shifted even farther to the red, at 702 nm. The resonance pathways containing 22 π bonds for both Cu(2-5) and Cu(2-6) diketo, exemplify this dramatic shifting by the lowering of the Q(0-0) transition energy.

Another prominent feature that these two chlorins exhibit was also observed in the OPP-THP optical spectra [33]. This is the increase in intensity of the Q_x band due to the cancellation of the degeneracy of the x-polarized transitions.

22 - π

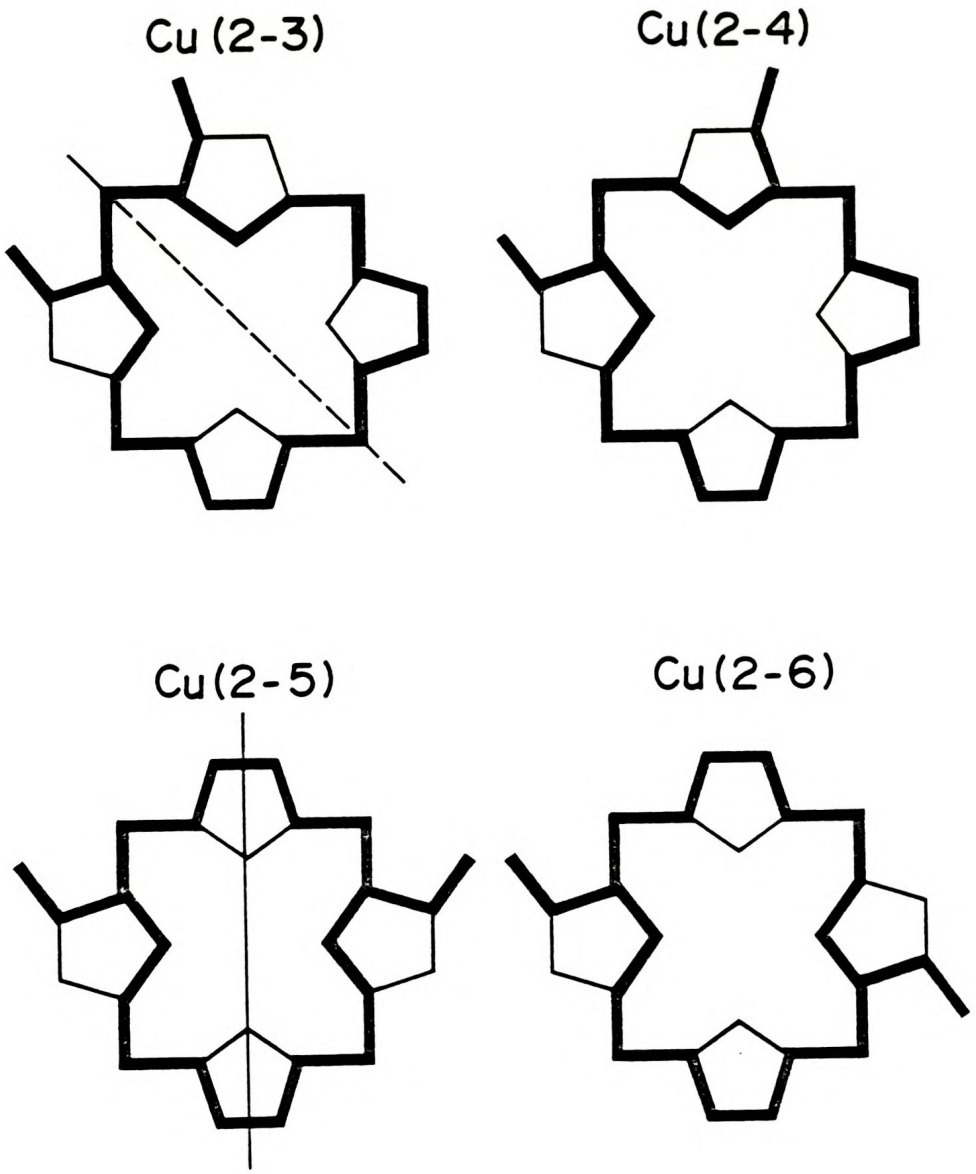

Figure 13. 22 π electron conjugation pathway.

B. RESONANCE RAMAN SPECTROSCOPY OF CHLORINS AND RELATED COMPOUNDS

1. Some general theoretical aspects

Raman spectroscopy has shown great resurgence during the past few decades with the development and use of lasers as monochromatic tunable radiation sources. It has been proven through the years that Raman spectroscopy can be a powerful tool for the understanding of electronic structure and molecular interaction, including application to such complicated systems as proteins [34,35,36,37]. Raman spectroscopy enjoys certain natural advantages over infrared spectroscopy, such as the possibility of working with glass or silica cells, weak scattering from H_2O, polarization studies, etc. [38].

Resonance Raman spectroscopy involves an experiment where the excitation wavelength, λ_{exc}, used corresponds to a molecular transition in the sample, i.e. the energy of the incident light approaches that of an absorption of the sample.

In general the total intensity I_{kn} of radiation scattered into a solid angle of 4π due to a Raman transition in a particular system is [39]:

$$I_{kn} = \frac{128\pi^5(\nu_0 \pm \nu_{kn})^4}{3c^4} \left| {}_{\rho}\Sigma_{,\sigma}(\alpha_{\rho\sigma})_{kn} \right|^2 I_0 \qquad (2.3)$$

where I_0, ν_0 are respectively the intensity and frequency of incident, exciting radiation, and $\nu_0 \pm \nu_{kn}$ is the

frequency of the scattered radiation, which we will abbreviate ν_L; where the (+) sign refers to anti-Stokes scattering and the (-) sign to Stokes scattering. Finally, $(\alpha_{\rho\sigma})$ is the $\rho\sigma$ Cartesian coordinate component of the polarizability tensor, and which relates the initial to the final eigenstates [40] according to:

$$\begin{matrix} P_x \\ P_y \\ P_z \end{matrix} = \begin{matrix} \alpha_{xx} & \alpha_{xy} & \alpha_{xz} \\ \alpha_{yx} & \alpha_{yy} & \alpha_{yz} \\ \alpha_{zx} & \alpha_{zy} & \alpha_{zz} \end{matrix} \begin{matrix} E_x \\ E_y \\ E_z \end{matrix} \qquad (2.4)$$

where P_i and E_i are the polarization i.e., induced dipole, and electric field respectively.

This scattering tensor takes the following form according to Kramers and Heisenberg-Dirac, being derived by a second order perturbation (dispersion) formula:

$$(\alpha_{\rho\sigma})_{kn} = \frac{1}{hc} \sum_m \frac{\langle k|\mu_\rho|m\rangle\langle m|\mu_\sigma|n\rangle}{\nu_{km} - \nu_0 + i\Gamma_m} + \frac{\langle n|\mu_\sigma|m\rangle\langle m|\mu_\rho|k\rangle}{\nu_{nm} + \nu_0 + i\Gamma_m}$$

where μ_σ, μ_ρ are the electric dipole moment operators; i.e., $\mu_\rho = -\sum_l e(S_l)_\rho$ and $(S_l)_\rho$ is the ρth component of the lth electron's position vector. Γ_m is the natural half-width of the state $|m\rangle$. The summation runs over all intermediate states $|m\rangle$, neglecting states $|k\rangle$ and $|n\rangle$.

In Equation (2.4) above, both terms in the brackets must be considered in the case where ν_0 is far from resonance, i.e., when $\nu_{km} - \nu_0 \gg 0$, whereas the energy

denominator of one vibronic manifold decreases, thus dominating the summation over states m, as resonance is approached.

One of the major challenges that many scientists [41,42,43] successfully met was the elucidation of the vibronic nature of the states and operators in the scattering tensor. For this purpose the adiabatic Born-Oppenheimer (ABO) approximation will be used [44], in which the vibronic states are formed as products of pure vibrational states $i(R_\xi)>$, with pure electronic states $|k(R_\xi,q)>$. R_ξ and q are the vibrational normal coordinates and the electronic coordinates respectively. Writing:

$$|k> = |k(R_\xi,q)>|i(R_\xi)>, \tag{2.5}$$

then

$$i(R_\xi) = \prod_\xi \psi_\xi(U_\xi) \tag{2.6}$$

where U_ξ is a set of normal coordinates and ψ_ξ are the harmonic oscillator eigenstates.

By substitution of the ABO approximation into Equation (2.4), $(\alpha_{\rho,\sigma})_{kg\to ki}$ for the resonance case becomes:

$$(\alpha_{\rho\sigma})_{kg\to ki} = \frac{1}{c} \sum_m \sum_w \frac{<i|\sigma_{km}|w><w|\rho_{km}|g>}{h\nu_{kg,ki} - h\nu_0 + i\Gamma_{mw}} \tag{2.7}$$

where

$$\rho_{km}(U) = \int k(U_\xi,q)\mu_\rho m(U_\xi,q)da \qquad (2.8)$$

and similarly:

$$\sigma^{(\upsilon)}_{km} = \int k(U_\xi,q)\mu_\sigma m(U_\xi,q)dq. \qquad (2.9)$$

Equations (2.8) and (2.9) both represent the electronic transition dipoles between the two electronic states $|k>$ and $|m>$ respectively.

Now expanding $\rho(U_\xi)$ or $\sigma(U_\xi)$ in a Taylor series about the equilibrium nuclear coordinates will enable us to perform the integration over these coordinates, i.e.,

$$\rho(U_\xi) = \rho(U)_{U=0} + \frac{\partial \rho(U)}{\partial U}_{U=0} + \ldots$$

$$= \rho + \rho' U_\xi + \ldots$$

After truncation and substitution of the above expression into Equation (2.7) we obtain:

$$(\alpha_{\rho\sigma})_{kg\to ki} = \sum_m \sum_w \sum_\xi (h\nu_{sw,kg} - h\nu_0 + i\Gamma_{mw})^{-1}$$

$$\times \rho^\circ_{km}\sigma^\circ_{mk}\langle i|w\rangle\langle w|g\rangle + \rho'_{km}\sigma^\circ_{mk}\langle i|U_\xi|w\rangle\langle w|g\rangle$$

$$+ \rho^\circ_{km}\sigma'_{mk}\langle i|w\rangle\langle w|U_\xi|g\rangle$$

$$+ \rho'_{km}\sigma'_{mk}\langle i|U_\xi|w\rangle\langle w|U_\xi|g\rangle \qquad (2.10)$$

where $\rho'_{km} = \left(\frac{\partial \rho(U_\xi)}{\partial U_\xi}\right)_{U=0}$, $\rho^\circ = \rho(U_\xi)_{U=0} = \rho(o)$.

The first term in the square brackets of Equation (2.10) above corresponds to the so called Albrecht A term [41] and the second and third terms (neglecting the fourth term as too small relative to them) correspond to the Albrecht B term.

As resonance is reached by simply allowing the energy $h\nu_0$ to approach $h\nu_{sw,kg}$, the denominator of expression (2.7) becomes extremely small, which makes $\alpha_{\rho\sigma}$ very large. Hence, when $h\nu_{sw,kg} - h\nu_0$ becomes of the order of a vibrational energy level difference, $h\omega$, then neglecting the dependence of the denominators on the excited state vibrational quantum numbers is no longer valid or appropriate.

Basically two types of expansions can be derived from Equation (2.10) (the expansion of the polarizability tensor), the Franck-Condon 0th order [45] and the Herzberg-Teller 1st order [46] perturbation terms. The former term involves no vibronic coupling and is the A-term mentioned previously, whereas the latter term involves vibronic coupling of states ρ'_{km}, σ'_{mk}, is called the B-term, and takes the form:

$$\rho'_{km} = \sum_{\xi} \sum_{p \neq m} \rho^{\circ}_{kp} \langle p | \frac{\partial H}{\partial u_{\xi}} | m \rangle (E_m - E_p)^{-1} \qquad (2.11)$$

where H is the Hamiltonian for the total electronic energy of the molecule, $|p\rangle$ corresponds to other than $|k\rangle$ and $|m\rangle$ states, and $\frac{\partial H}{\partial U_{\xi}}$ is the vibronic coupling operator [47].

The mixing of states by this operator depends upon the energy separation between these states and upon the relative coupling strength of $\langle p|\frac{\partial H}{\partial U_\xi}|m\rangle$.

The form that α takes now is:

$$(\alpha_{\rho\sigma})_{kg\rightarrow ki} = \frac{1}{c}\Sigma \; h\nu_{sw,kg} - h\nu_0 + i\Gamma_{mw}^{-1} \; \rho'_{km}\sigma^{\circ}_{mk}$$

$$\times\langle i|u_\xi|w\rangle\langle w|g\rangle \qquad (2.12)$$

Now substituting the expression for ρ'_{km} into the above expression we obtain:

$$(\alpha_{\rho\sigma})_{kg,ki} = \frac{1}{c}\sum_m\sum_w \frac{\rho_{km}\sigma_{mk}\langle i|w\rangle\langle w|g\rangle}{h\nu_{kg,mw} - h\nu_0 + i\Gamma_{mw}}$$

$$+ \sum_m\sum_{p\neq m}\sum_w \frac{\langle p|\frac{\partial H}{\partial U_\xi}|m\rangle\langle E_m - E_p\rangle^{-1}}{h\nu_{m,p}(h\nu_{kg,mw} - h\nu_0 + i\Gamma_{mw})}$$

$$\times \rho_{km}\sigma_{mk}\langle i|w\rangle\langle w|U_\xi|g\rangle + \sigma_{mk}\rho_{pk}\langle i|U_\xi|w\rangle\langle w|g\rangle$$

where the first term is the A-term and the second and third the B-term again.

Far from resonance, the F-C vibrational integrals could take the form:

$$\frac{1}{c}\sum_w \frac{\langle i|w\rangle\langle w|g\rangle}{h\nu_{kg,mq} - h\nu_0 + i\Gamma_{mw}} \qquad \alpha\langle i|g\rangle = \delta_{g,i}. \qquad (2.13)$$

The above term signifies the application of closure to the F-C vibrational integrals far from resonance, where the A-term contributes only to Rayleigh scattering; closure

vanishes as the resonance denominator is affected by the vibronic energy separations.

The F-C overlap integrals for Raman scattering become non-zero with the removal of orthogonality between a ground state vibrational level and an excited state level with a different vibrational quantum number [38]. Hence, the orthonormality of the vibrational levels is preserved and the F-C integrals give rise to Rayleigh scattering even at resonance, if and only if, along some particular coordinate, the potential curve for nuclear vibration in the excited electronic state can be obtained from that for the ground state; this is accomplished by a translation along the energy axis by a purely electronic excitation energy. Therefore, the removal of orthogonality and the occurrence of Raman-scattering may be due to: a) the shift in equilibrium position upon excitation and b) a difference in vibrational frequency between the ground and excited states.

In reference to preceding Equation (2.12) large scattering intensities are affected by a strong intrinsic transition moment, σ°_{mk}, where the modes enhanced in resonance are those most responsible for a "forbidden" intensity contribution in an allowed electronic band. This is true in the case where the H-T term dominates the scattering mechanism, which implies that totally symmetric modes are enhanced when two allowed electronic bands of the same symmetry vibronically couple.

2. Resonance Raman results

The resonance Raman spectra of Cu(OEC), Cu(2F-6F), Cumonoketo, Cu(2-3), Cu(2-4), Cu(2-5), Cu(2-6), and Cu(α-γ) in CH_2Cl_2 upon excitation at 406.7 nm are shown in Figures 14 through 21.

The Raman lines between 1500 and 1750 cm^{-1} appear to be most enhanced, with the exception of Cu(α-γ) where the lower frequency lines between 600 and 800 cm^{-1} and 1300-1500 cm^{-1} are most enhanced.

In previous studies the high frequency bands above 1400 cm^{-1} were found to contain significant $C_\alpha C_m$, C_β-C_β and $C_\alpha C_\beta$ contributions [48,49]. The band at 1580-1590 cm^{-1} was found to be mostly due to the C_β-C_β stretching [50,51]. Also, the band between 1620-1650 cm^{-1} was found to contain a great deal of $C_\alpha C_m C_\alpha$ contribution. In the present study we will focus our attention primarily on the carbonyl stretching frequency itself. We will also investigate the effect of the position of the carbonyl around the pyrrole rings, and its implications on the resonance Raman spectra. Assignment of the various other bands at this point cannot be made without normal coordinate analysis (NCA) [52,53]; thus it will be omitted.

The Cu(OEC) Raman spectrum exhibit no bands above 1650 cm^{-1}, where the carbonyl stretch is expected. This is due to the absence of a C=O group on the ring, as illustrated in Figure 14.

Figure 14. RR spectra of Cu (OEC). λ exc. = 413.1 nm

1100

The Cu(2F-6F) spectra, however, exhibit a low intensity band at 1671 cm^{-1}, as shown in Figure 15. This band is attributed to the H-C=O stretching frequency itself. Lutz [54] observed a similar line at 1664 cm^{-1} in the type b chlorophyll spectra which he also assigned to the C=O stretching of the formyl group. A similar line was observed by Gradyushko, et al. [55], and by Fischer, et al. [56] for the type b chlorophylls. Kitagawa [27] recently reported a similar line around 1650-1670 cm^{-1} in the RRS of monoformyl and diformyl iron protoporphyrin IX. This Raman line, as noted earlier, is assignable to the formyl C=O group stretching mode and corresponds to the characteristic line of reduced cytochrome oxidase at 1670 cm^{-1} observed by Salmeen, et al. [26]. The stretching frequency of the C=O bond depends on the delocalization of the formyl π electrons to the porphyrin ring which affects the bond order of the C=O bond. Thus the higher the delocalization of the formyl π electrons to the porphyrin the less the bond order and hence the lower the stretching frequency. This effect is observed on going from Cu(2F-6F) to (2F-4F) iron protoporphyrin IX, to chlorophyll b.

The Cumonoketo spectra, as illustrated in Figure 16a, b exhibit a broad band at 1710 cm^{-1}. A similar band was also observed by Lutz [54] in chlorophyll b spectra between 1695-1705 cm^{-1} which he assigned to the ketone C=O stretching motion. We assign the band at 1710 cm^{-1} to the same motion.

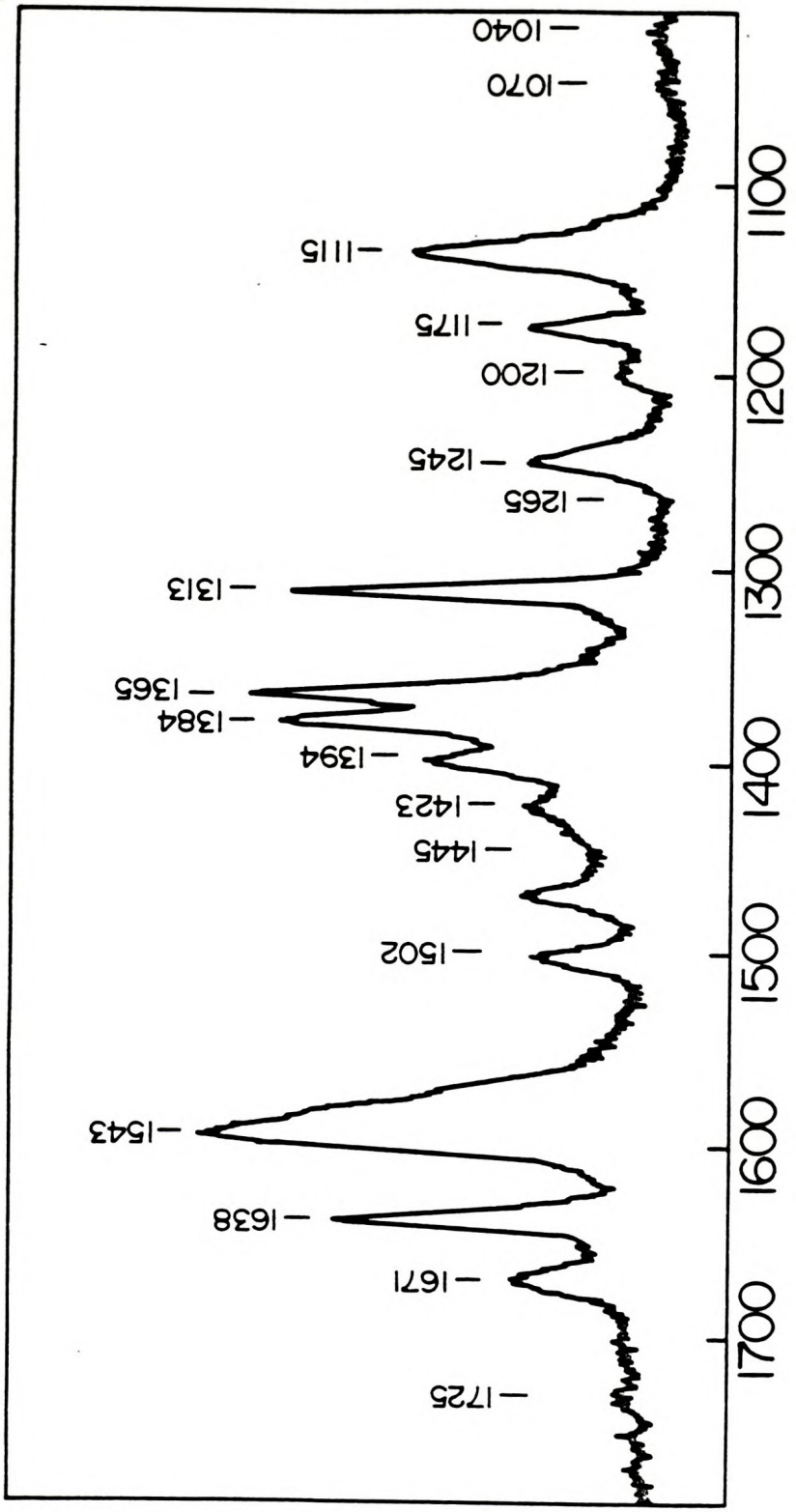

Figure 15. RR spectra of Cu(2F-6F). λexc. = 413.1 nm.

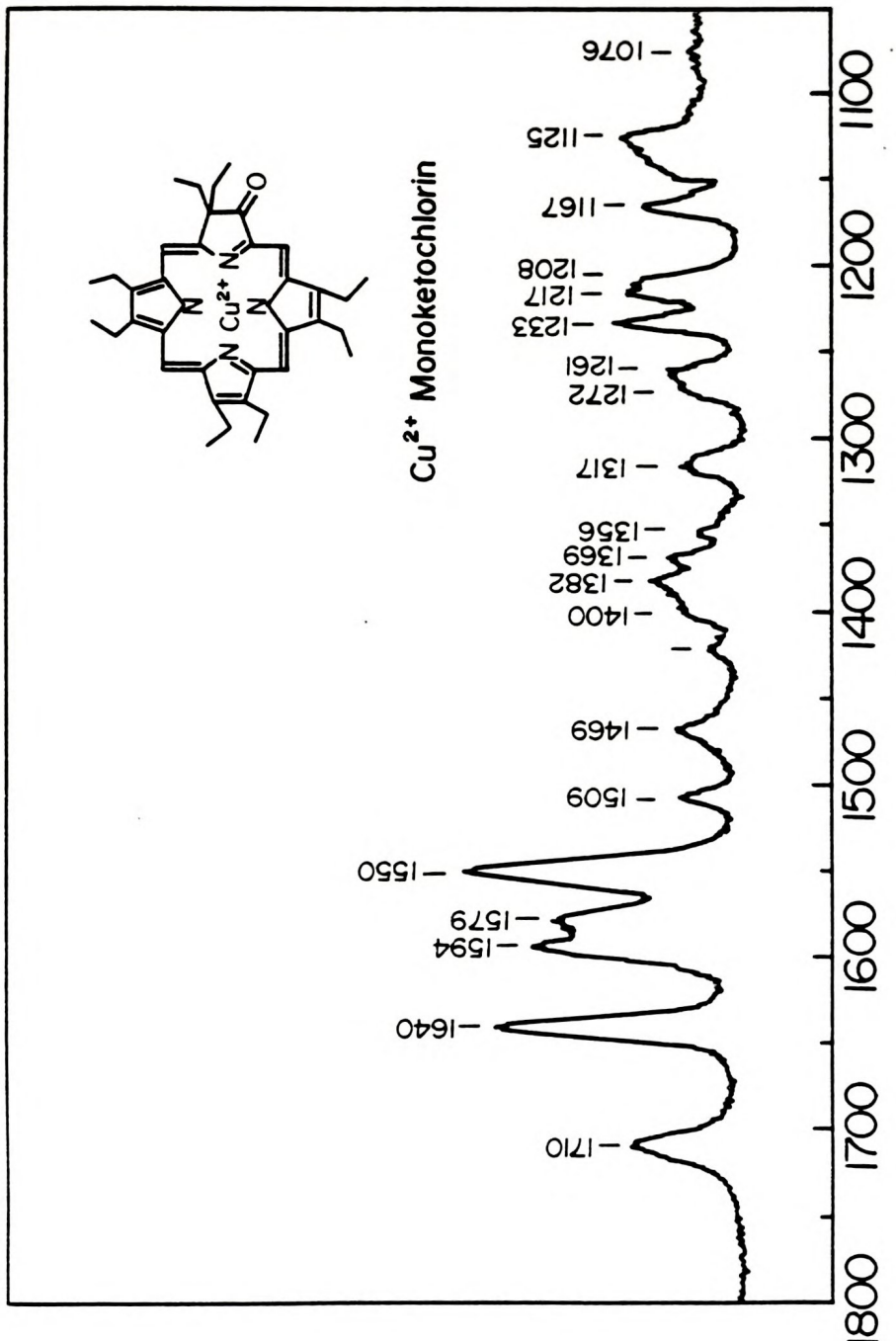

Figure 16a. RR spectra of Cu monoketo. λexc. = 406.7 nm.

100
3502
2511
1361

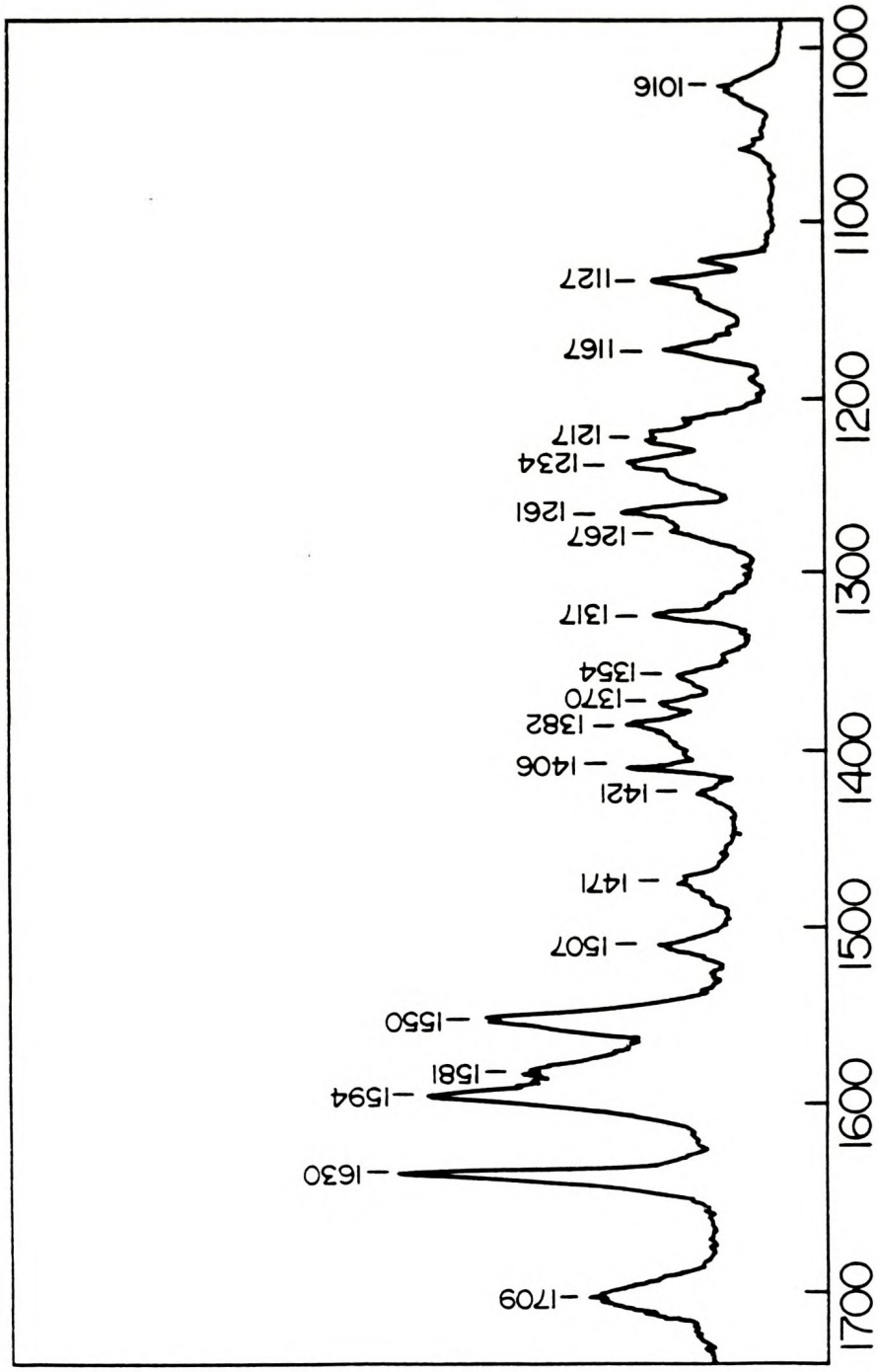

Figure 16b. RR spectra of Cu monoketo. λexc. = 413.1.


0001
0011
1100

The Cu(2-3) spectra are shown in Figure 17a, b. A prominent feature is the band at 1705 cm^{-1} which is again assigned to the carbonyl stretching motion. This band is broad and appears symmetric which indicates that the two carbonyls on positions 2 and 3 are symmetrically located; i.e. there is a mirror plane in the molecule as shown in Figure 22.

On the contrary, the Cu(2-4) spectra as shown in Figure 18 exhibit a highly unsymmetrical band at 1718 cm^{-1}, which corresponds to the C=O stretching frequency. The fact that this band is unsymmetrical suggests that the two carbonyls are non-equivalent and that there is no mirror plane through the molecule as seen in Figure 22.

Similarly, the Cu(2-6) spectra illustrated in Figure 20 show a very broad unsymmetrical band at 1700-1708 cm^{-1} which again indicates the non-equivalence of the two carbonyls and the lack of a mirror plane in the molecule.

However, the Cu(2-5) spectra, as shown in Figure 19 exhibit a low intensity rather symmetrical broad band at 1707 cm^{-1} assignable to the carbonyl stretching motion. This indicates again that the two carbonyls are equivalent, due to the presence of a mirror plane as shown in Figure 22.

Finally, the Cu(α-γ) spectra show absolutely no scattering above 1650 cm^{-1} (see Figure 21) for reasons that are at the present unknown to us. We also checked the region where -OH stretching occurs (3000-4000 cm^{-1}), in case enolization of C=O via hydrogen bonding occurred

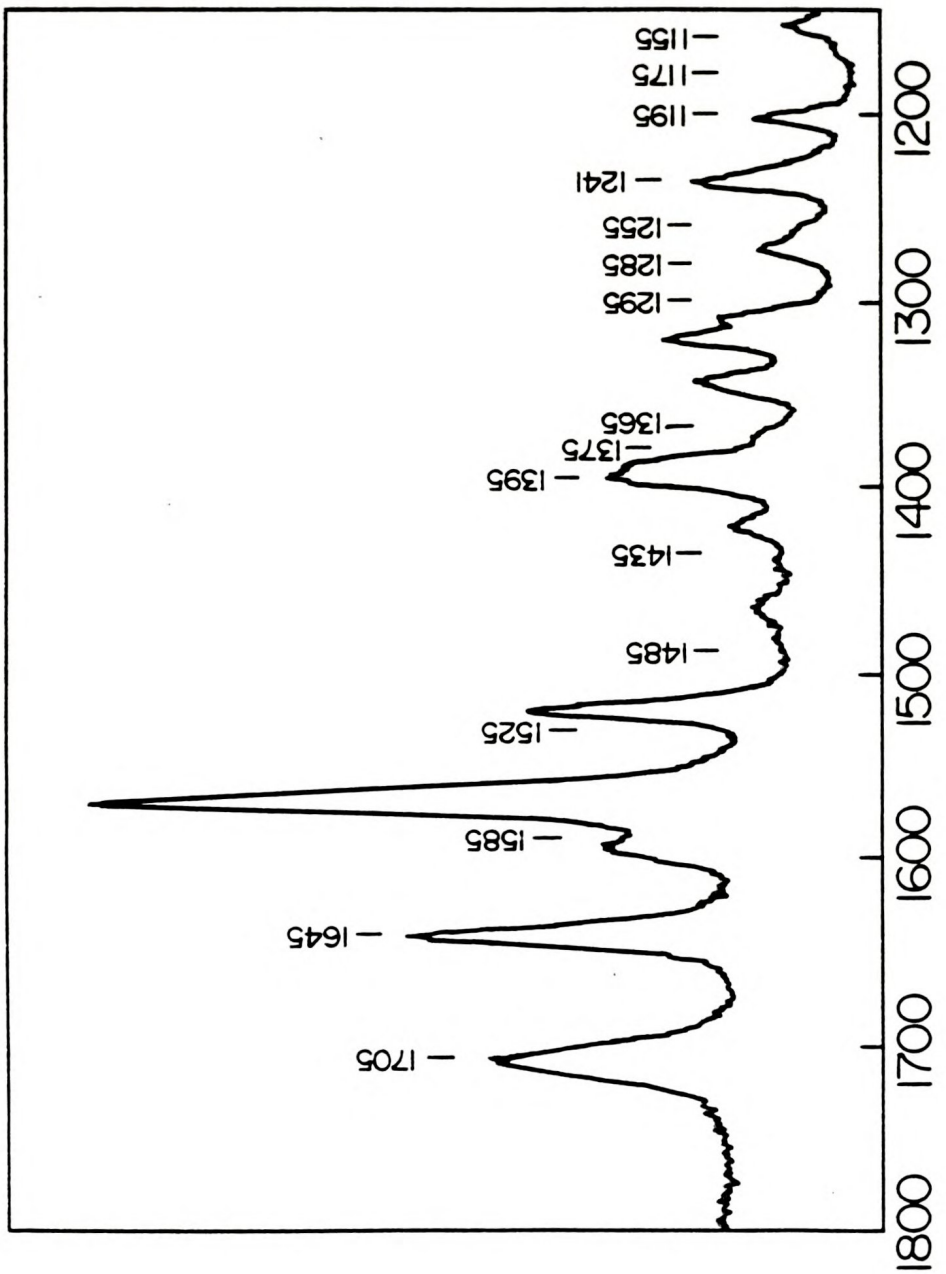

Figure 17a. RR spectra of Cu (2-3) diketo. λ exc. = 406.7 nm.

ISCO

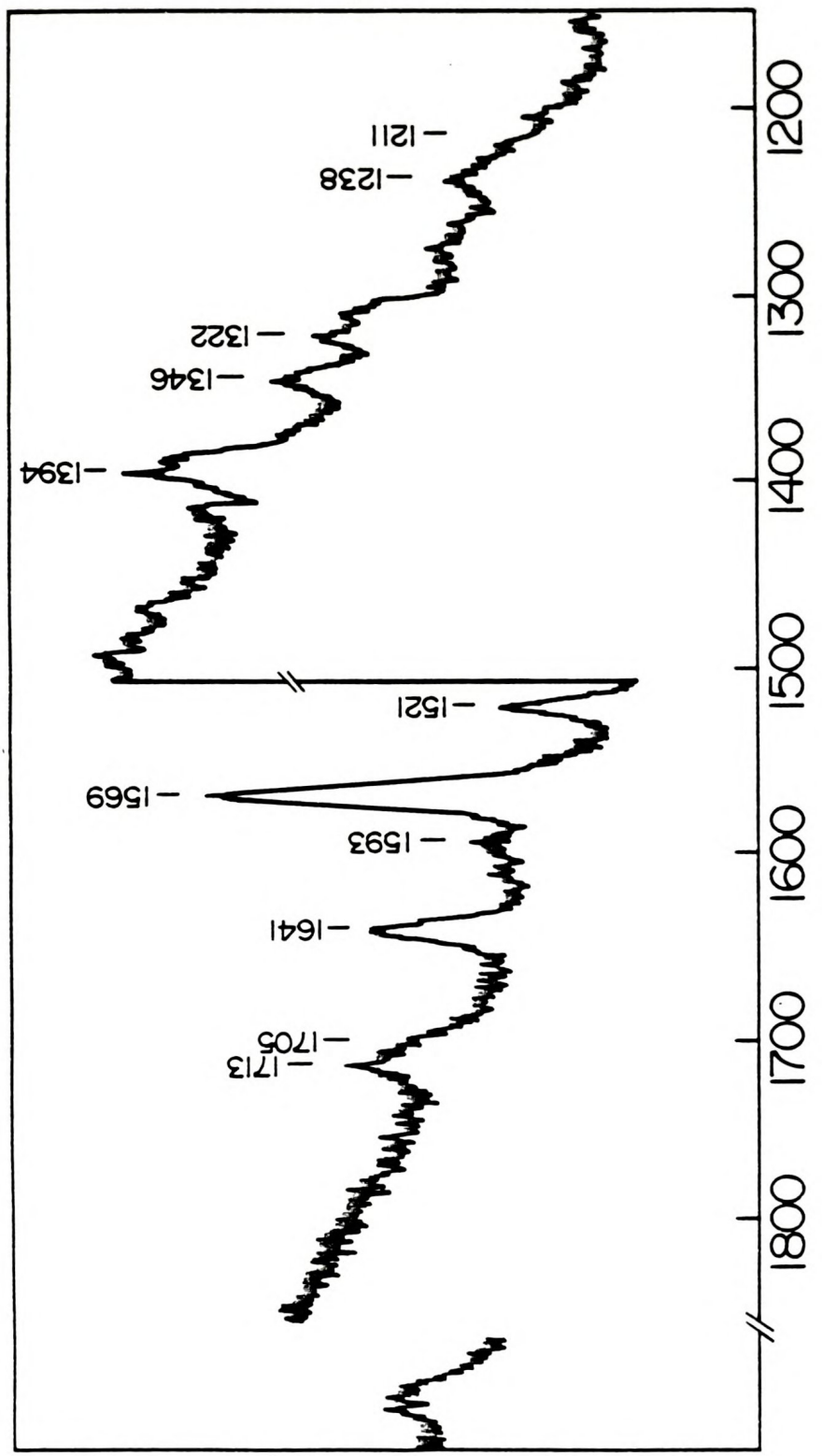

Figure 17b. RR spectra of Cu(2-3). λexc. = 413.1 nm.

Figure 18. RR spectra of Cu (2-4) diketo.

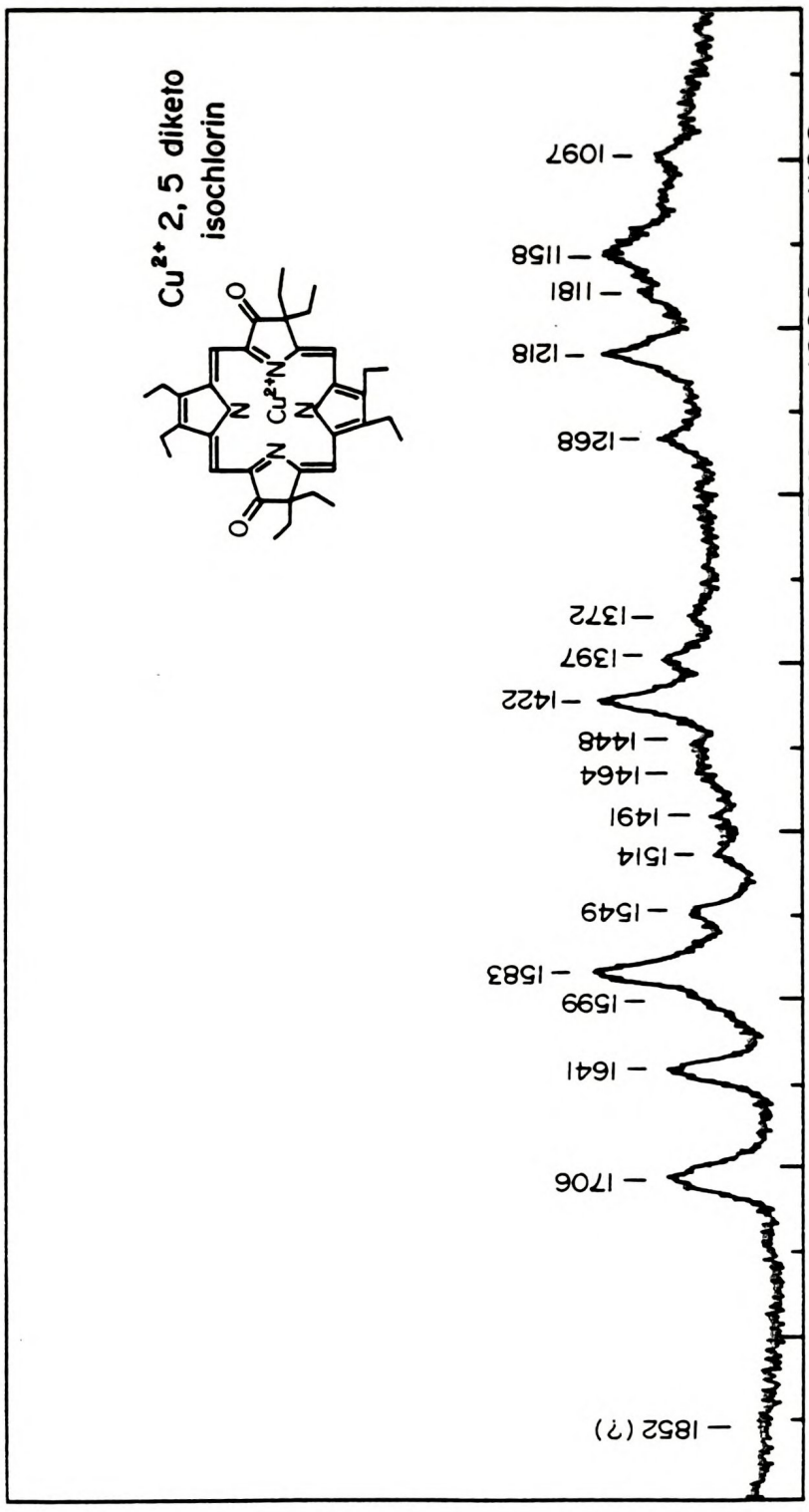

Figure 19. RR spectra of Cu (2-5) diketo.

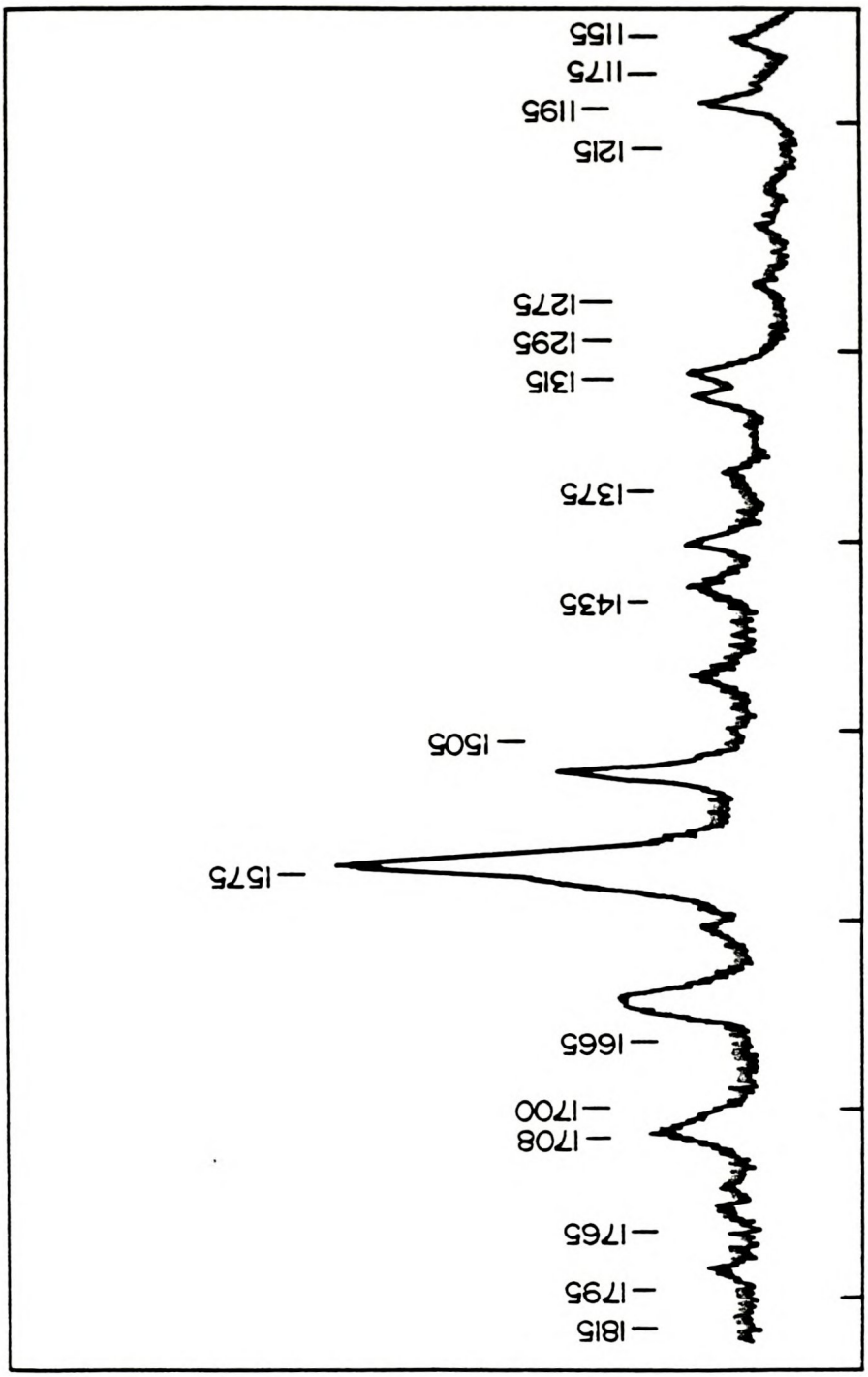

Figure 20. RR spectra of Cu(2-6) diketo. λexc. = 406.7 nm.

1500

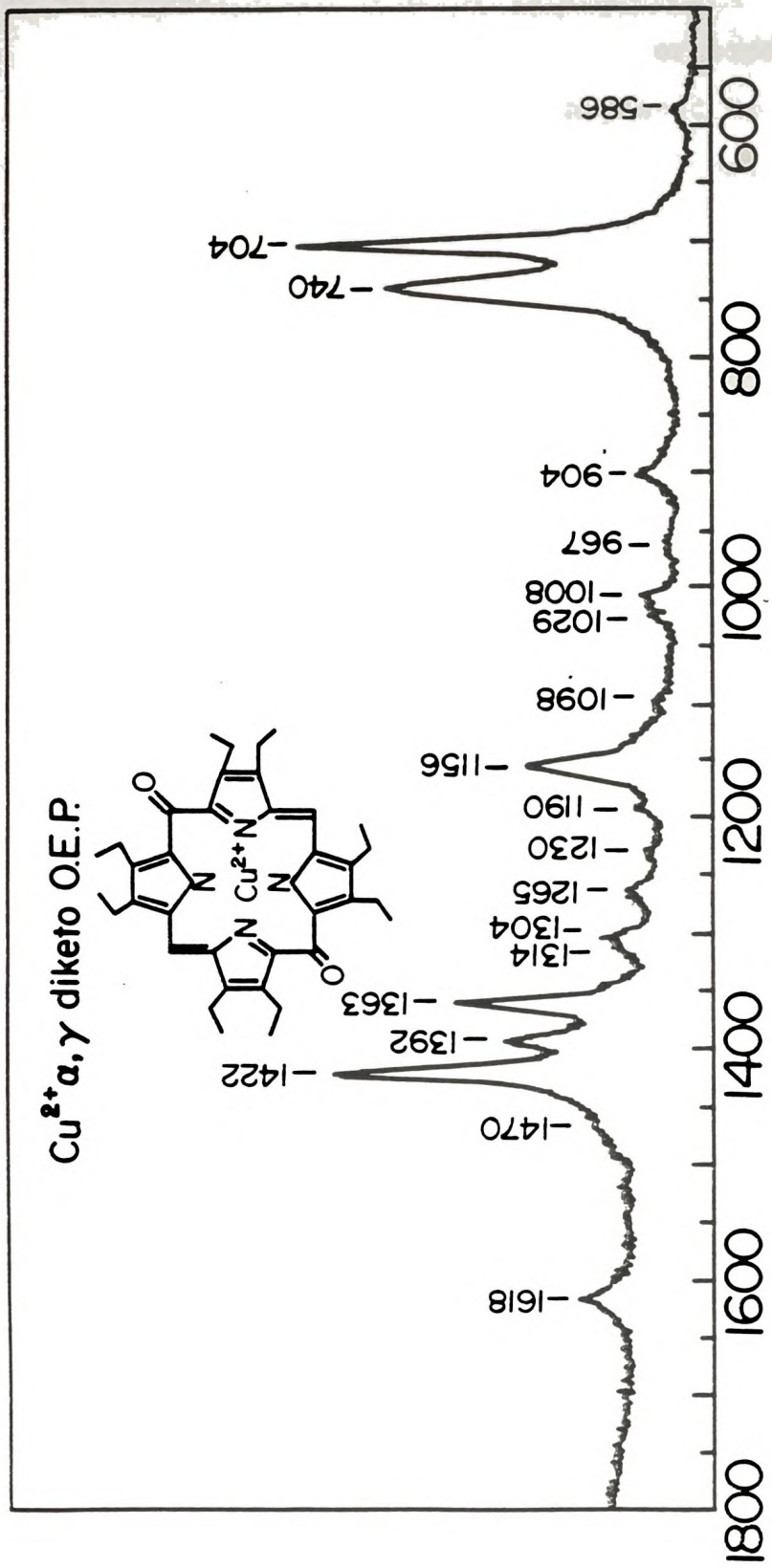

Figure 21. RR spectra of Cu (α-γ) dimeso diketo.

during preparation of the sample, and again no signal was detected.

Upon excitation at 413.1 nm the corresponding Raman lines for Cumonoketo and Cu(2-3) appeared at 1710 and 1710 cm^{-1} respectively. The spectra for the remaining chlorins with λ_{exc} = 413.1 nm were not recorded in the present study.

Let us now examine how the position of the exciting line effects the relationship of the absorption spectra to the observed Raman vibrational frequencies (see Table 2).

The Cumonoketo spectra exhibit a uniform enhancement pronounced in both the high and low frequency modes. The Cu(2-3) spectrum exhibits enhancement of the modes around 1300 cm^{-1} and mainly towards the higher frequency region. The Cu(2-4) and Cu(2-6) spectra show enhancement of the modes around 1100 cm^{-1} (middle region) in resonance with the Soret (λ max. = 426 nm). The most prominent feature of the latter spectrum is the high intensity of the bands around 1500-1600 cm^{-1} and the uniformity of the remaining high and low frequency modes. Finally, in the Cu(2-5) spectrum under λ_{exc} = 406.7 nm with λ_{max} = 442 nm the high frequency modes around 1960 cm^{-1} should be enhanced in resonance with the Soret. The spectrum though between 1100-1700 cm^{-1} appears to be uniform.

TABLE 2 - $\Delta\bar{\nu}$ values under Soret excitation.

λ_{exc} = 406.7 nm

Cu(OEC)	Cumono	Cu(2-3)	Cu(2-4)	Cu(2-5)	Cu(2-6)
$\Delta\bar{\nu}^{\dagger}$=-412 cm^{-1}	$\Delta\bar{\nu}$ =492 cm^{-1}	$\Delta\bar{\nu}'^{\dagger\dagger}$=1333 cm^{-1} $\Delta\bar{\nu}$ =1964 cm^{-1}	$\Delta\bar{\nu}$ =1114 cm^{-1}	$\Delta\bar{\nu}'$ =1964 cm^{-1} $\Delta\bar{\nu}$ = 779 cm^{-1}	$\Delta\bar{\nu}$ =1114 cm^{-1}

λ_{exc} = 413.1 nm

$\Delta\bar{\nu}^{\dagger}$=-793 cm^{-1}	$\Delta\bar{\nu}$ =111 cm^{-1}	$\Delta\bar{\nu}'$ = 953 cm^{-1} $\Delta\bar{\nu}$ =1583 cm^{-1}	* ----	* ----	* ----

†The negative value is indicative of preresonance enhancement.

††The prime indicates a split Soret and signifies the maximum peak (λ max).

*Spectra have not been recorded.

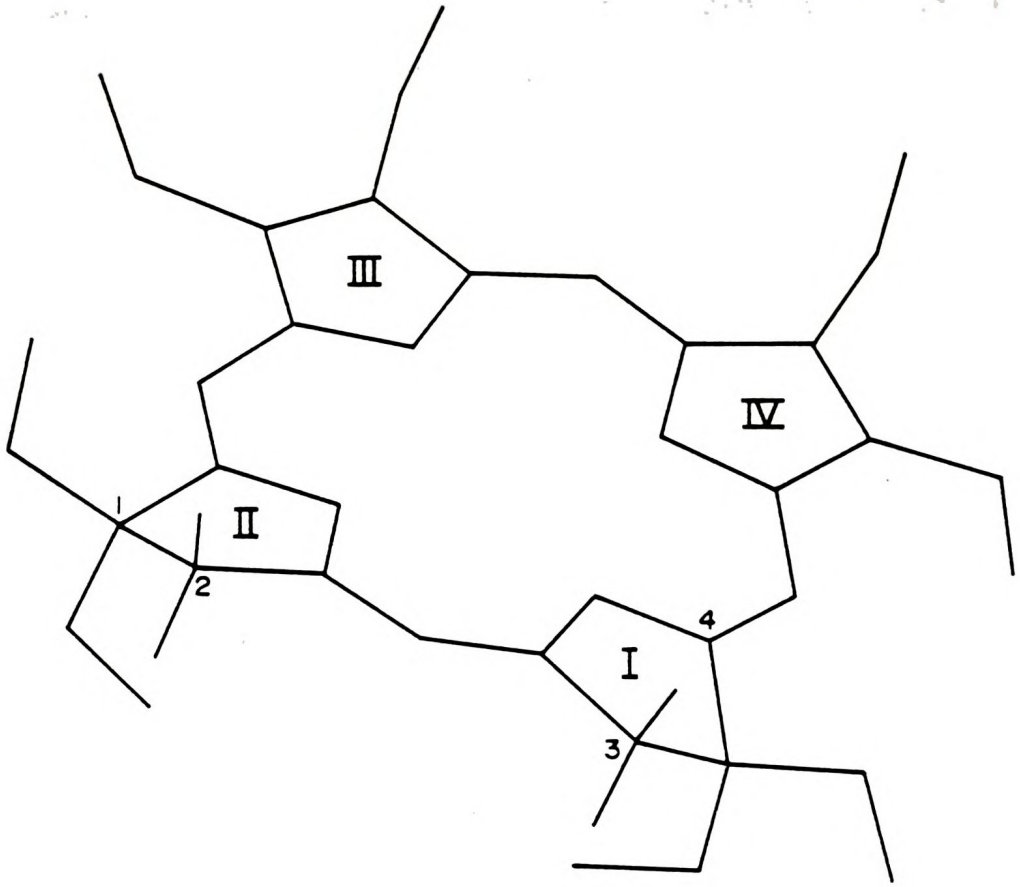

Figure 22. Structure of isobacteriochlorin

C. INFRARED SPECTROSCOPY - RESULTS

Infrared spectroscopy has received some attention as a means of determining the physicochemical properties of various metal chelates of porphin [57,58], TPP [59,60], OEP [61,62], etc. In all these cases the recorded spectra serve mainly to characterize the compounds investigated, rather than to deduce bonding and structural information.

Ogoshi, et al. [61] have taken infrared spectra of metalloporphins and performed normal coordinate analysis. They concluded that the bands between 1700-950 cm^{-1} correspond to C-H in plane bending, C-C stretching, C-N stretching, CCN in plane bending, as well as various coupled vibrations between these modes. Earlier, Thomas and Martell [59,60] performed studies on metal chelates of TPP and found that the bands near 1000 cm^{-1} may be associated with M-N vibrations and that the bands near 350 cm^{-1}, 530-550 cm^{-1}, and 970-920 cm^{-1} of metal chelates of protoporphyrin IX are metal sensitive.

We have also employed infrared spectroscopy as a means for specifically detecting the carbonyl signal(s). Our infrared spectra support and verify the results of our resonance Raman spectra.

The Cumonoketo, Cu(2-3), Cu(2-5) and Cu(2F-6F) spectra (shown in Figures 23a,b,d,f) gave a single sharp band at 1710, 1709, 1707 and 1670 cm^{-1} respectively, differing by 0, 0, +1, and 0 cm^{-1} from their corresponding resonance Raman counterparts. The sharp band in each case between

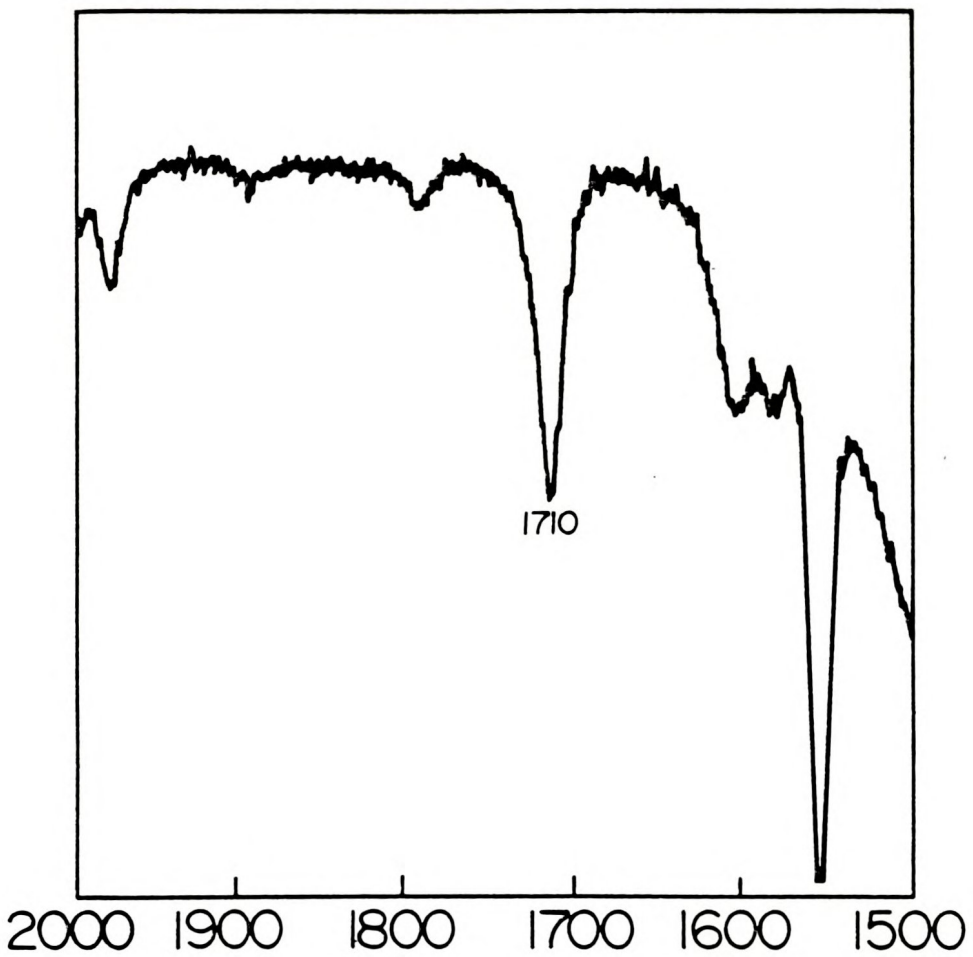

Figure 23a. IR spectra of Cu (monoketo).

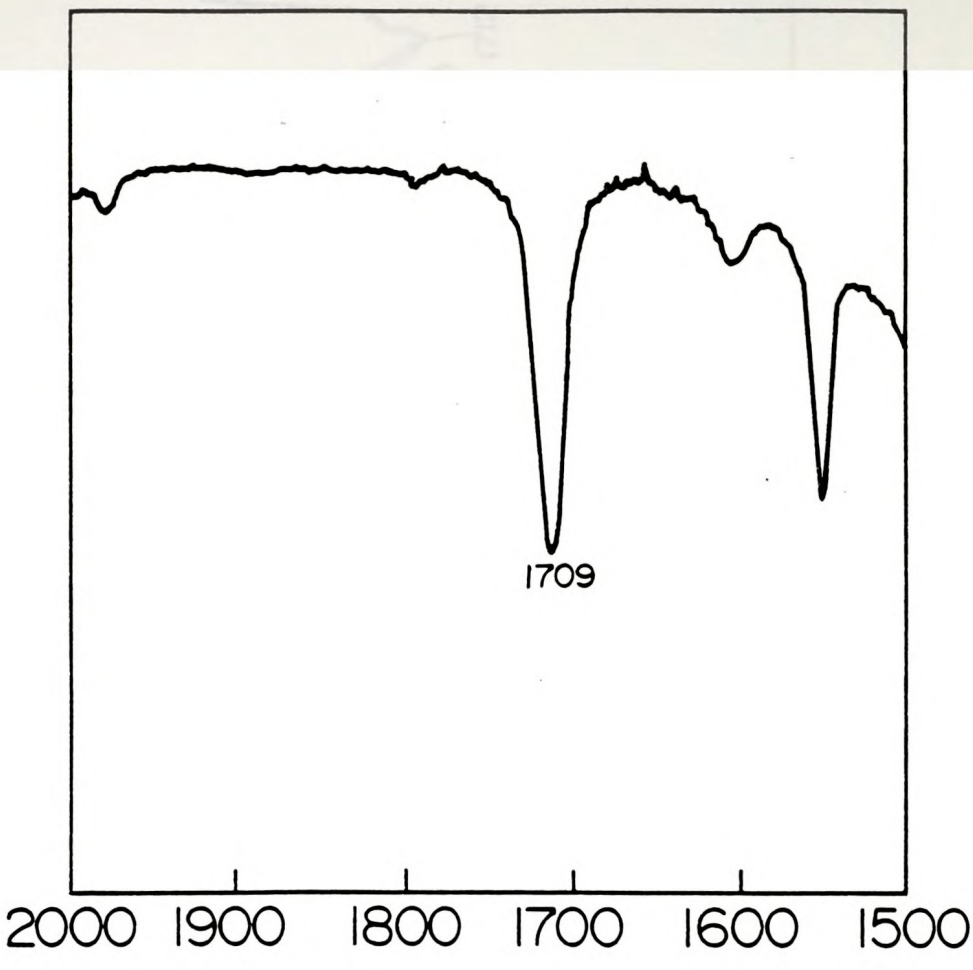

Figure 23b. I-R spectra of Cu (2-3)

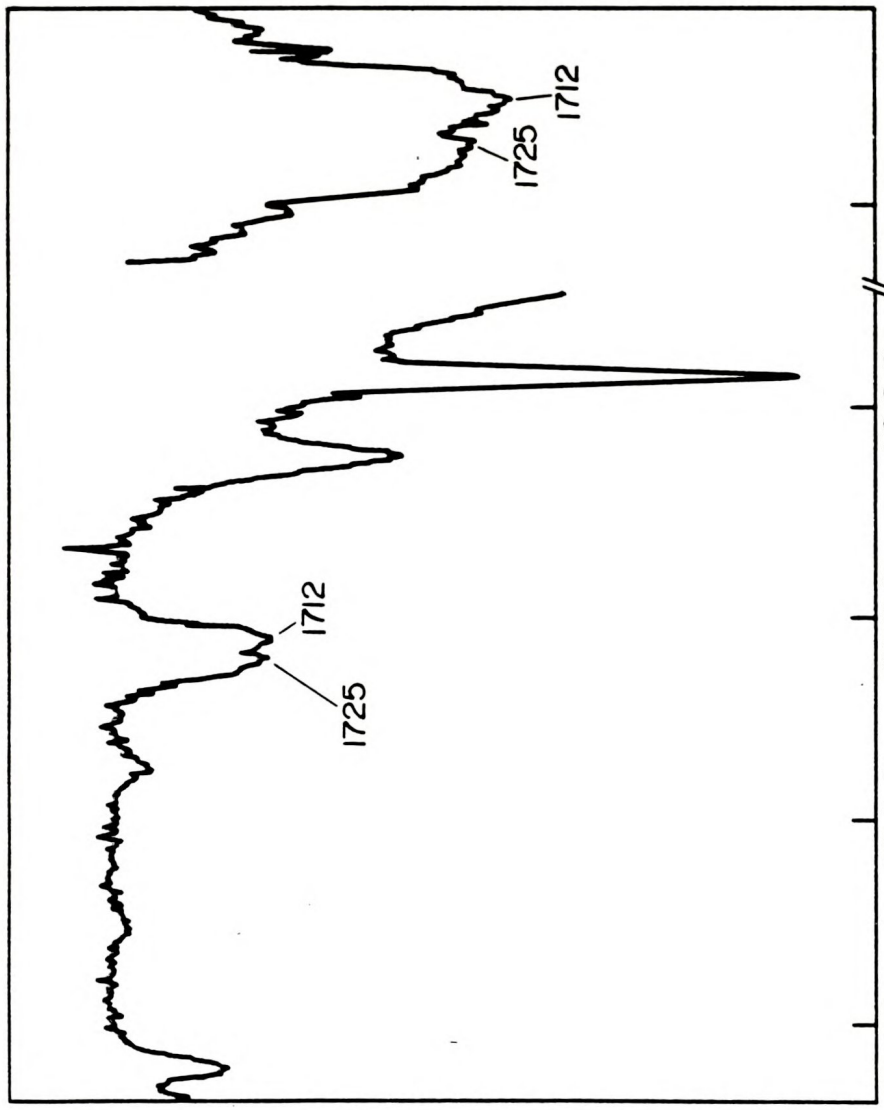

Figure 23c. I-R spectra of Cu (2-4).

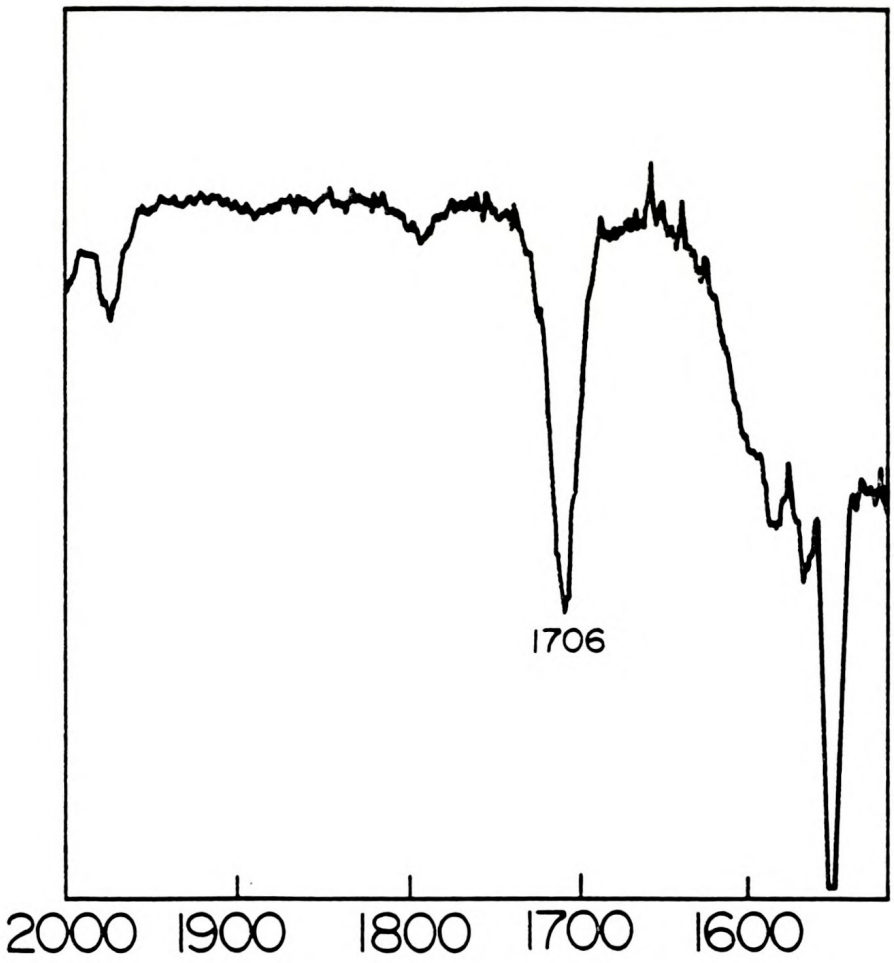

Figure 23d. I-R spectra of Cu (2-5)

1670-1710 cm^{-1} signifies the presence of a mirror plane of symmetry in the molecule and the equivalence of the two carbonyls.

On the other hand, the infrared spectra of Cu(2-4), and Cu(2-6), as illustrated in Figures 23c and 23e show a broad split band at 1712 cm^{-1} and 1725 cm^{-1} for the former and at 1700 cm^{-1} and 1706 cm^{-1} for the latter. These carbonyl stretching frequencies differ by ± 2 cm^{-1} from their resonance Raman counterparts. (For purposes of comparison, the experimental results are summarized in Table 3.)

Finally, the Cu (α-γ) infrared spectrum showed neither carbonyl nor hydroxyl signals. Thus we conclude that the dimeso compound should be re-investigated.

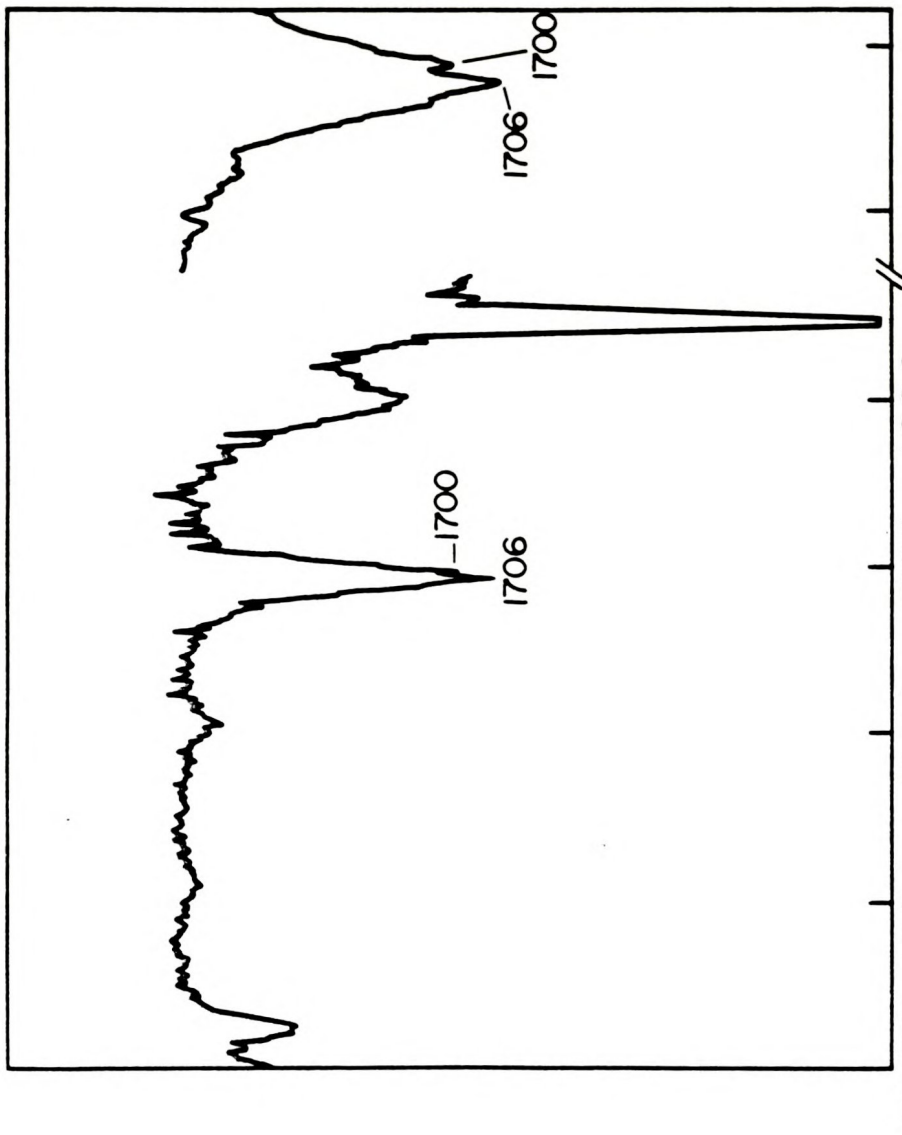

Figure 23e. I-R spectra of Cu(2-6)

VOC

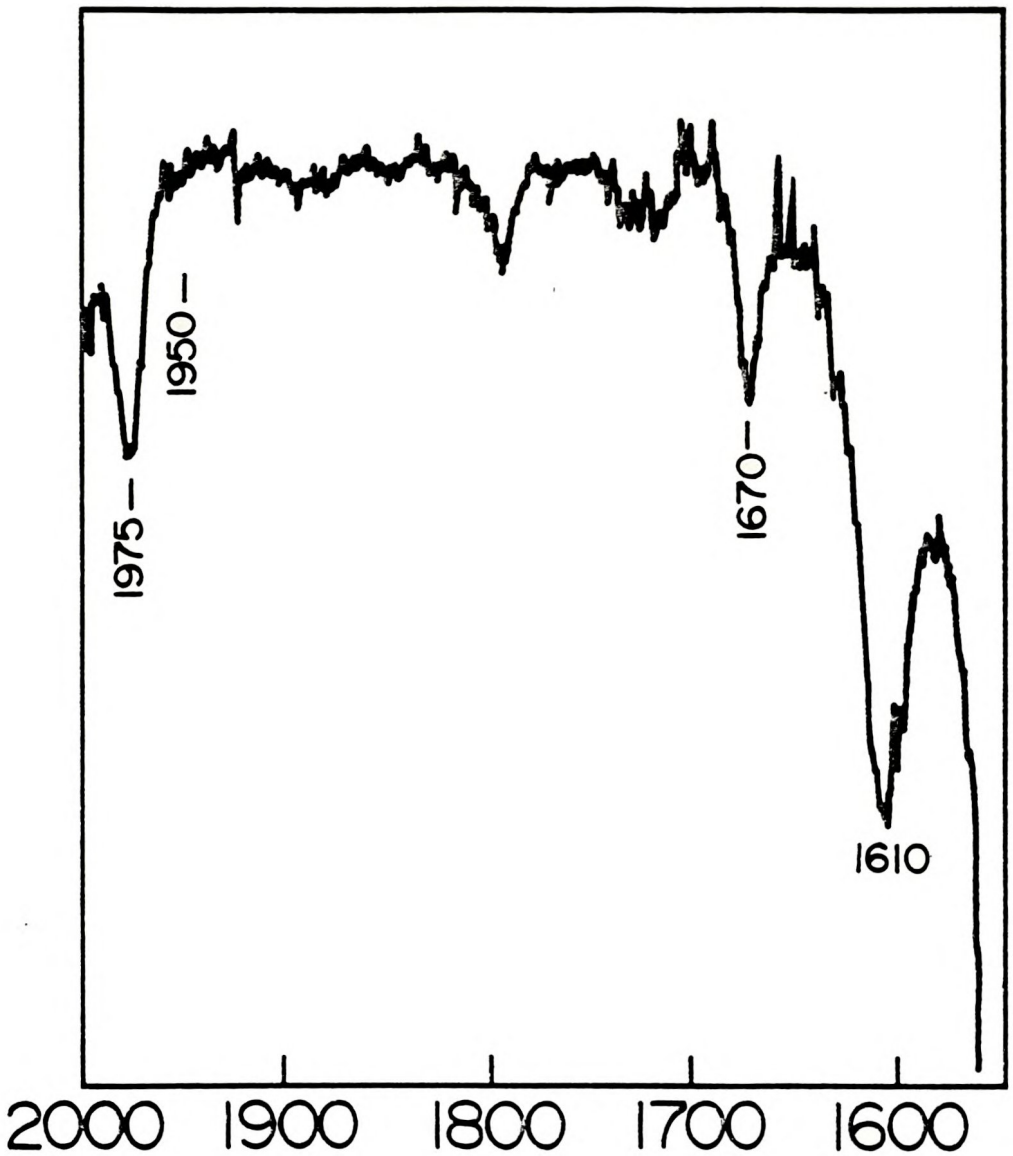

Figure 23f. IR spectra of Cu (2F - 6F).

TABLE 3 - Energies of the carbonyl signals in both I.R. and RRS.

	I·R	λ_{exc} = 406.7 nm	λ_{exc} = 413.1 nm
Cu mono	1710 cm^{-1}	1710 cm^{-1}	1709 cm^{-1}
Cu(2-3)	1709 cm^{-1}	1709	1710 cm^{-1}
Cu(2-4)	1712 cm^{-1}	1720 cm*	----
	1725 cm		
Cu(2-5)	1706 cm^{-1}	1707 cm^{-1}	----
Cu(2-6)	1700 cm^{-1}	1700 cm^{-1}*	----
	1706 cm^{-1}	1708 cm^{-1}	
Cu(2F-6F)	1670 cm^{-1}	----	1670 cm^{-1}
Cu(α-γ)	absent	absent	absent

*asymmetrical band

---- indicates that the corresponding value has not been recorded.

D. COMPARISON OF RESONANCE RAMAN BANDS OF Cu(OEC) UPON EXCITATION AT 413.1 NM WITH THOSE OF OZAKI, ET AL. AT λ_{EXC} = 488.0 NM AND OTHER MODELS.

The resonance Raman spectra of Cu(OEC) in CH_2Cl_2 upon excitation at 413.1 nm and 488.0 nm are shown in Figure 24. Within experimental uncertainty, most of the Raman bands were not shifted, but new lines appeared under Soret excitation. These lines fall at 1141, 1171, 1232, 1275, and 1293 cm^{-1}. The Raman lines at 703, 741, 1400, 1583, and 1643 cm^{-1} were the most prominent, in contrast to the spectrum recorded by Ozaki, where the strongest scattering was observed between 1100-1300 cm^{-1}. The Raman lines between 1300-1650 cm^{-1} appeared to be the most enhanced upon excitation at 413.1 nm. (A careful excitation profile is needed to determine the excitation wavelength at which intensity enhancement is the strongest.) Another very important characteristic of our spectra compared to those of Ozaki, et al. is the decrease in overall intensity, and the very intense low frequency bands at 741 cm^{-1} and 703 cm^{-1} upon excitation at 413.1 nm. In Ozaki's spectra, also, the 1643 cm^{-1} band is the most prominent, but in our spectra the 1583 cm^{-1} band is the most prominent. The peak positions and relative intensities of the α-β- and Soret-excited Raman spectra of Cu(OEC) are listed in Table 4.

The molecular structure of Cu(OEC) is shown in Figure 25, where we also define the Cartesian coordinate system.

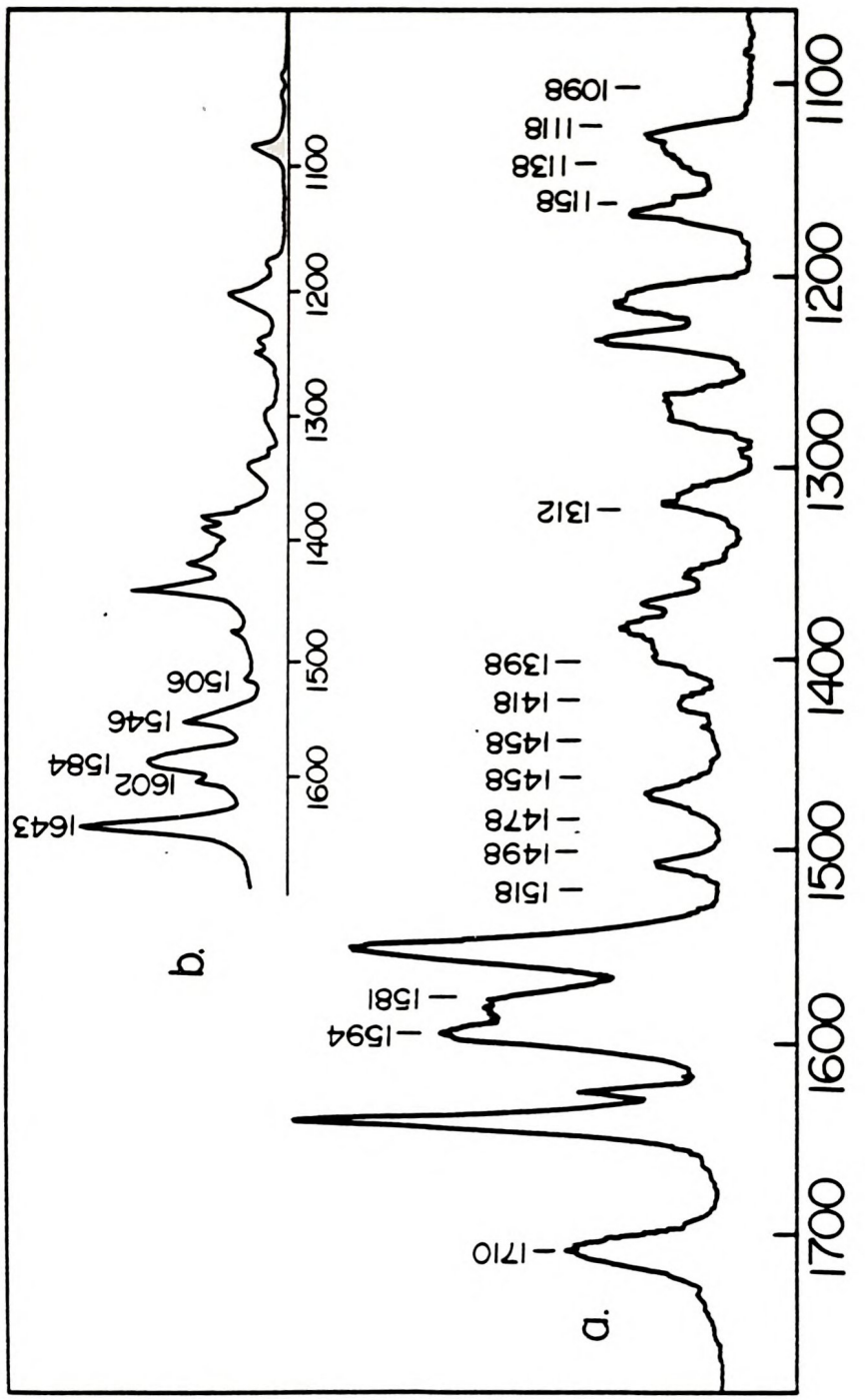

Figure 24a. RR spectra of Cu monoketo. λexc. = 413.1 nm.
b. " " " " " = 488.0 nm.

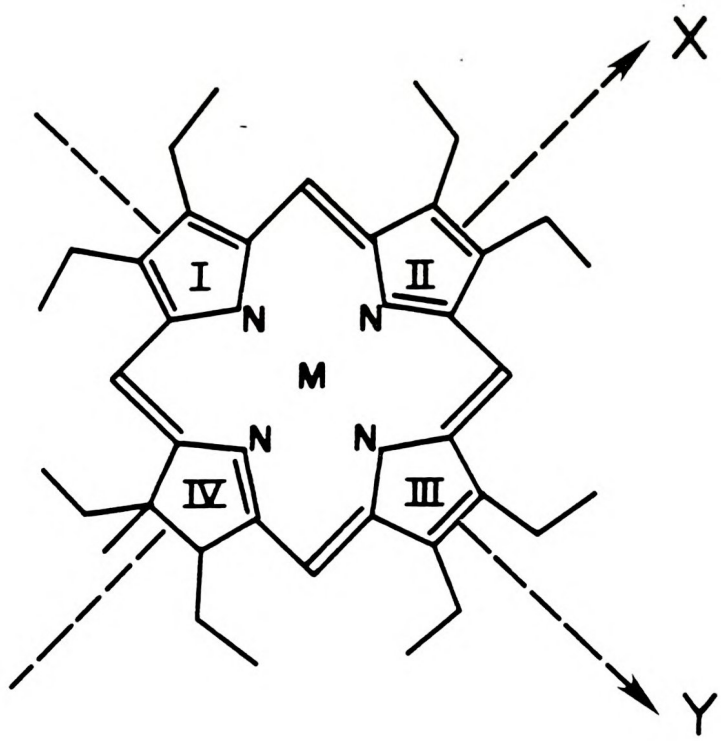

Figure 25. Chemical structure of metallo-trans-octaethylchlorin. (from ref. # 61)

TABLE 4 - RRS peak positions and intensities of the Cu(OEC) bands under Soret and visible excitation.

VISIBLE*		SORET	
Band Position	I_{band} †	Band Position	I_{band}
	I_{1424}		I_{1423}
1023	0.28	1020	0.20
1129	0.19	1130	0.37
		1141	0.69
1154	0.43	1156	0.60
		1171	0.40
1199	0.19		
1211	0.24	1210	0.26
		1232	0.43
1264	0.19	1262	0.46
		1275	0.51
		1293	0.57
1314	0.34		
1362	0.55	1357	0.69
1372	0.52	1371	0.74
1390	0.47	1390	0.94
1402	0.66	1400	1.00
1424	1.00	1423	1.00
1464	0.38	1464	0.34
1506	0.33	1507	0.43
1546	0.65	1544	0.66
1584	0.86	1583	1.14
1602	0.57	1598	0.97
1643	1.24	1643	0.80

*Values taken from Reference

†Ratio of the intensity of each Raman line to the intensity of the solvent Raman line.

Due to the lowering of symmetry - from D_{4h} to C_{2v} - by the reduction of a double bond in one pyrrole ring for Cu(OEC) (see Figure 25) we have a totally different picture from that of Cu(OEP) with regard to the vibrational modes. The A_{1g} and B_{1g} vibrations of M(OEP) as illustrated in Table 5, being symmetric to the C_2 axis, give rise to the totally symmetric A_1 modes of Cu(OEC). Similarly, the antisymmetric modes A_{2g} and B_{2g} give rise to the non-totally symmetric B_2 modes. A consequence of the above is the expectation of more bands group theoretically for Cu(OEC) than for Cu(OEP) due to the lowering of symmetry.

According to Ozaki, there are eight $C_\alpha C_m$ stretching vibrations -$4A_1$ + $4B_2$- for Cu(OEC); four of them are extremely weak since they correspond to the E_u mode in D_{4h} symmetry. Three of the most obvious modes of this type are observed at 1643, 1583, and 1507 cm^{-1} upon excitation at 413.1 nm, being shifted by 0, -1, and +1 cm^{-1} respectively from their counterparts under 488.0 nm excitation. The Raman lines of Cu(OEC) at 1130, 1156, 1357, and 1371 cm^{-1} correspond to these of Ozaki at 1129, 1157, 1362, and 1372 cm^{-1} which showed frequency shifts upon ^{15}N substitution. These lines, which also appear in the Ni(OEP) spectra [49] at 1121, 1159, 1348, and 1383 cm^{-1} and which also showed ^{15}N isotopic frequency shifts, were assigned to the C_α-N stretching modes. The Cu(OEC) bands at 1598 and 1544 cm^{-1} upon excitation at 413.1 nm are shifted by -4 and -2 cm^{-1} respectively under 488.0 nm excitation. These lines

Cu (OEP)		Cu (OEC)
D_{4h}		C_{2v}
A_{1g}, B_{1g}	symmetric to C_2 axis	A_1 modes
A_{2g}, B_{2g}	anti-symmetric to C_2 axis	B_2 modes

TABLE 5. from Ref. # 61.

Symmetry correlation between C_{2v} and D_{4h} groups for the in-plane vibrations.

Cu (OEP)

correspond to those of Ni(OEP) at 1602 cm^{-1} and 1576 cm^{-1} which were assigned to the C_β-C_β stretching mode.

Lutz, et al. [54] studied the resonance Raman spectra of chlorophyll and its isotopically substituted derivatives. The Raman lines of chlorophyll a at 1115, 1147, 1290, 1350 and 1380 cm^{-1} recorded by Lutz are consistent with the lines of Cu(OEC) which fall at 1130, 1156, 1293, 1362 and 1371 cm^{-1}. The small differences in frequency may be attributable to differences in the peripheral substituents, the central atom, and/or the number of reduced rings.

Thus it becomes obvious that under preresonance enhancement for λ_{exc} = 413.1 nm both the low and high frequency modes are enhanced and the spectrum appears more or less uniform.

CHAPTER 3

Conclusions

The results obtained from the application of a variety of spectroscopic methods to chlorins, isochlorins and isobacteriochlorins have been described in the preceding chapter. These methods provide insight into the structure of the molecules and offer help to others who study similar compounds.

This chapter serves as a synopsis of the involvement of the carbonyl moiety in the compounds investigated, in an effort to provide a consistent picture of each molecule. Three major aspects are summarized:

1. Absorption spectra
2. Resonance Raman spectra
3. Infrared spectra

1. Absorption spectra

The most prominent feature of the optical spectra of all the carbonylated derivatives of chlorin is the shifting to the red of both the Soret and Q bands (as in cytochrome oxidase [26]) due to the presence of the electron-withdrawing ketone group. This effect is most notably observed in the Cu(2-6), Cu(2-3) and Cu(2-4) diketo spectra, where the visible band can be clearly distinguished at 702, 688, and

688 nm respectively; in Cu(OEC) the Q band maximum lies at 615 nm. This tremendous shift towards lower energy indicates lifting of the degeneracy of the e_g states. The effect of carbonylation on the Soret band is rather hard to distinguish because the latter is multiply split.

The Cumonoketo spectra project a different and less dramatic picture than the compounds mentioned above. The $Q_y(0\text{-}0)$ band appears minimally red shifted, at 618 nm. This is an indication that the carbonyl mono-substitution causes little apparent perturbation on the ring with respect to the energy of the $Q_y(0\text{-}0)$ transition. The Soret also appears to be split for both Cumonoketo and Cu(OEC), but with a higher degree of splitting for the former, which indicates the presence of an electron withdrawing group. This less dramatic red shifting can be attributed to the smaller conjugation pathway (involving 20 π bonds) for Cumonoketo in comparison to the disubstituted ketoporphyrins.

In contrast, carbonyl disubstitution causes more extensive effects (see Figure 22) which are translated as a skewing in the structure of the molecule. This effect is more obvious for Cu(2-4) and Cu(2-6) diketos as was revealed by RRS and IRS.

2. Resonance Raman spectra

The presence or absence of the ketone vibrational band(s) was interpreted in terms of the involvement or non-involvement of the C=O in the conjugation pathway of the ring.

The most prominent feature of the diketo Raman spectra is the broadness of the C=O band, which indicates the presence of both carbonyls. The Cu(2-4) and Cu(2-6) diketo spectra gave the broadest C=O signal. Recently, Tsubaki, et al. [27] showed that when both positions 2 and 4 are occupied by formyl groups, donation of electrons from the individual C=O groups becomes less than in the case of monosubstitution, probably due to mutual repulsion of the electrons. The C=O groups may possibly have a similar stretching frequency, giving rise to one broad band. Indeed, a single C=O stretching frequency was observed, at higher wavenumber (1668 cm^{-1}) than either of the absorptions for mono-substitution at position 2 or 4 (1648 and 1660 cm^{-1} respectively). This effect is clearly shown in the spectrum of Cu(2F-6F) (1661 cm^{-1}), and also in the spectrum of Cu(2-4) diketo, where the carbonyl signal is at 1720 cm^{-1} which is higher than the signal for Cumonoketo which is at 1710 cm^{-1}.

The carbonyl signal for Cu(2-4) and Cu(2-6) diketos also appeared to be split in the Raman spectra, which indicates non-equivalence of the two carbonyls. This non-equivalence of the two carbonyls for each molecule can be translated into the ring as a higher degree of perturbation of these structures in the form of skewing or bending, and the lack of a mirror plane through these molecules. (Note, however, that the splitting for Cu(2-6) is much less dramatic due to the C_2 axis which makes the two carbonyls

"interchangeable".)

The two marker bands for C_β-C_β and $C_\alpha C_m C_\alpha$ stretching are worthy of special mention. The C_β-C_β stretching frequency is normally found between 1580-1590 cm^{-1} [50,51]. In our Raman spectra, this band fluctuates greatly (16 cm^{-1}) which indicates a varying pattern of perturbation from one molecule to the other.

The methine bridge, $C_\alpha C_m C_\alpha$ stretching frequency appears to be approximately the same for each molecule (1640-1646 cm^{-1}). This could indicate a slight or negligible perturbation of the methine bridge by the carbonyl mono- or disubstitution at the C_β-C_β bond. The frequency difference is largest between Cumonoketo and Cu(2-3) diketo in comparison to the remaining diketos.

When all the above postulations are considered one may see that the structure-sensitive region (above 1500 cm^{-1}) primarily is perturbed under carbonyl mono- or disubstitution. This region includes $C_\alpha C_m C_\alpha$, C_β-C_β and $C_\alpha C_\beta$ stretching vibrations.

3. Infrared spectra

Infrared spectroscopy was employed in order to specifically detect the carbonyl band(s) and to supplement resonance Raman spectroscopy. In this regard IRS proved to be very fruitful. The bands for Cumonoketo, Cu(2-3), Cu(2-5) and Cu(2F-6F) were broad but not split, whereas the bands for Cu(2-4) and Cu(2-6) were doubly split. The splitting signified the non-equivalence of the carbonyls

and also the structural differences between the molecules.

Suggestions for Further Research

Although all the vibrational spectra recorded during this project are of good quality, additional work is needed for further justification of our results. More Soret excitation lines should be utilized and a resonance Raman excitation profile should be obtained in order to accurately determine which Raman lines are resonance enhanced. Isotopic (^{15}N, ^{17}O) substitutions should be made in order to clearly distinguish the various vibrational stretching frequencies of the various bonds such as C=O, C_α-N, C_β-C_β, etc. Different metals should also be used such as Sn, which will tell us which bands are metal sensitive. (A detailed and complete normal coordinate analysis should be also performed for specific assignment of each spectroscopic line to a normal mode.) Finally, the Cu(2-4) diketo and Cu(α-γ) dimeso must be reinvestigated due to the anomalies observed in their spectra, which we attributed to impure samples.

LIST OF REFERENCES

LIST OF REFERENCES

1. Gouterman, M., in "The Porphyrins", Vol. III, (Dolphin, D. ed), pp. 1-165 (1978), Academic Press.

2. Lutz, M., Spectroscopy Letters, 7, 133-145 (1974).

3. Gurinovitch, G.P., Sevchenko, A.N., Solovyov, K.N., "Spectroscopy of Chlorophyll and Related Compounds", Izdatel'stvo Nauka; Tekhnika: Minsk, 1968 (English translation; AEC-TR-7199).

4. Moffitt, W., J. Chem. Phys., 22, 320, (1954).

5. Simpson, W.T., J. Chem. Phys., 17, 1218 (1949).

6. Platt, J.R., "Radiation Biology", A. Hollander, ed. Vol. III, Chapter 2, McGraw Hill, New York, 1956.

7. Gouterman, M., J. Chem. Phys., 30, 1139 (1959).

8. Ksenofontova, N.M., Solovyov, K.N., Tsenter, M.Y., Bobovich, Y.S., Shkirman, S.F., and Kachura, T.F., Zh. Prikl. Spektr., 17, 918 (1972).

9. Gouterman, M., Journal of Molecular Spectroscopy, 6, 138 (1961).

10. Shelnutt, J.A., "A simple interpretation of Raman excitation spectra of metalloporphyrins", to be published.

11. Ozaki, Y., Kitagawa, T., and Ogoshi, H., Inorganic Chem., 18, 1772 (1979).

12. Spiro, T.G., Accts. Chem. Res., 339 (1974).

13. Spiro, T.G., and Strekas, T.C., Proc. Nat. Acad. Sci. USA, 69, 2622 (1972).

14. Verma, A.L., and Bernstein, H.J., J. Chem. Phys., 61, 2560 (1974).

15. Solovyov, K.N., Ksenofontova, N.M., Shkirman, S.F., and Kachura, T.F., Spec. Lett, 6, 455 (1973).

Bibliography

16. Weiss, Jr., Charles, J. Mol. Spec., 44, 37 (1972).

17. Platt, J.R., J. Chem. Phys., 19, 263 (1951).

18. Platt, J.R., Klevens, Modern Physics, 16, 182 (1944).

19. Weiss, C., Kobayalshi, H., and Gouterman, M. J. Mol. Spec., 11, 108 (1963).

20. McHugh, A., Gouterman, M., and Weiss, C., Theor. Chim. Acta, 24, 346 (1972).

21. Goedheer, J.C., and Siero, P.J., Photochem. Photobiol., 6, 509 (1967).

22. Knop, J.V., and Stichtenoth, H., Z. Naturforsch., 27A, 639 (1972).

23. Sundbom, M., Acta. Chem. Scand., 22, 1317 (1968).

24. Caughey, W.S., Deal, R.M., Weiss, C., and Gouterman, M., J. Mol. Spec., 16, 451 (1965).

25. Weiss, C., and Gouterman, M., J. Chem. Phys., 43, 1838 (1965).

26. Babcock, G.T., and Salmeen, I., Biochemistry, 18, 2493 (1979).

27. Tsubaki, M., Nagai, K., and Kitagawa, T., Biochemistry, 19, 379 (1980).

28. Seely, G.T., and Calvin, M., J. Chem. Phys., 23, 1068 (1955).

29. Coyne from Reference #16.

30. Houssier, C., and Sauer, K., Biochim. Biophys. Acta, 172, 492 (1969).

31. Houssier, C., and Sauer, K., J. Amer. Chem. Soc., 92, 779 (1970).

32. Briat, B., Schooley, D.A., Recordo, R., Bunnenberg, E., and Djerassi, C., J. Amer. Chem. Soc., 89, 6170 (1967).

33. Longuet-Higgins, H.C., Rector, C.W., and Platt, J., J. Chem. Phys., 18, 1174 (1950).

34. Spiro, T.G., and Strekas, T.C., J. Amer. Chem. Soc., 56, 338 (1974).

35. Spaulding, L.P., Chang, C.C., Nai-Teng, Y., and Felton, R.H., J. Amer. Chem. Soc., 97, 2517 (1975).

36. Shelnutt, J.A., Rousseau, D.L., Friedman, J.M., and Simon, S.R., Proc. Natl. Acad. Sci., 76, 4409 (1979).

37. Ondrias, Mark R., Ph.D. Thesis, Michigan State University, 1980.

38. Robin, J.H., Clark, and Stewart, B., Structure and Bonding, 36 (1979).

39. Tang, J., and Albrecht, A.C., in "Raman Spectroscopy", Vol. 2 (Szymanski, H.A., ed), pp. 33-69, (1970), Plenum Press.

40. Guillory, W.A., in "Introduction to Molecular Structure and Spectroscopy", (Allyn and Bacon, Boston, 1977).

41. Albrecht, A.C., J. Chem. Physics, 33, 156 (1960).

42. Nafie, L.A., Pezolet, M., and Peticolas, W.L., Chemical Physics Letters, 20, 4043 (1976).

43. Shelnutt, J.A., O'Shea, D.C., Yu, N.T., Cheng, L.D., and Felton, R.H., J. Chem. Phys., 64, 1156 (1976).

44. Born, M., and Huang, K., in "Dynamical Theory of Crystal Lattices", (Oxford, 1956).

45. Condon, E.W., Phys. Rev., 32, 858 (1928).

46. Powell, J.L., and Crasemann, B., in "Quantum Mechanics", (Addison-Wesley, Massachusetts, 1961).

47. Levine, I.N., in "Quantum Chemistry", (Allyn and Bacon, Boston, 1970).

48. Kitagawa, T., Ozaki, Y., Kyogoku, Y., Adv. Biophys., 11, 153 (1978).

49. Abe, M., Kitagawa, T., Kyogoku, Y., J. Chem. Phys., 69, 4526 (1978).

50. Kitagawa, T., Abe, M., Ogoshi, H., J. Chem. Phys., 69, 4516 (1978).

51. Felton, R.H., Yu, N.T., O'Shea, D.C., and Shelnutt, J.A., J. Am. Chem. Soc., 96, 3675 (1974).

52. Bright, E., Wilson, Jr., J.C., Decius, J.C., and Cross, P.C., in "Molecular Vibrations", (Dover Publications, New York, 1955).

53. Mackintosh, D.F., Michaelian, K.H., Can. J. Spec., 24, 1 (1979).

54. Lutz, M., J. Ram. Spec., 2, 497 (1974).

55. Gradyushko, A.T., Mashenkov, V.A., and Solovyev, K.N., Biophysics, 14, 869 (1969).

56. Fischer, M.S., Templeton, D.H., Zalkin, A., and Calvin, M., J. Am. Chem. Soc., 94, 3613 (1972).

57. Mason, S.F., J. Chem. Soc., 976 (1958).

58. Ogoshi, H., Saito, Y., and Nakamoto, K., J. Chem. Phys., 57, 4194 (1972).

59. Thomas, D.W., and Martell, A.E., J. Am. Chem. Soc., 78, 1338 (1956).

60. Thomas, D.W., and Martell, A.E., J. Am. Chem. Soc., 81, 5111 (1959).

61. Ogoshi, H., Masai, N., Yoshida, Z., Takemoto, J., and Nakamoto, K., Bull Chem. Soc., Japan 44, 49 (1971).

62. Burger, H., Burczyk, K., and Fuhrhop, J.H., Tetrahedron, 27, 3257 (1971).